Late Neogene to Early Quaternary climate evolution in southwestern Europe from a continental perspective

Lope Ezquerro[1,†,*], Arsenio Muñoz[1], Carlos L. Liesa[1], José L. Simón[1] and Aránzazu Luzón[1]

[1] Departamento de Ciencias de la Tierra, Facultad de Ciencias, Grupo Geotransfer-Instituto de Investigación en Ciencias Ambientales (IUCA), Universidad de Zaragoza, Pedro Cerbuna 12, 50009, Zaragoza, Spain

[†] GEOBIOTEC, Department of Earth Sciences, NOVA School of Science and Technology, Campus de Caparica, P-2829 516 Caparica, Portugal.

* Corresponding author: Lope Ezquerro (lopezquerro@gmail.com)

Abstract

Paleoclimate reconstructions are mostly based on continuous oceanic records, but continental records, controlled by global and regional conditions, are paramount in identifying long- and short-term climatic variability between regions and investigating forcing mechanisms. Here we present a high-resolution lacustrine log from a western Mediterranean intramountain basin; it is based on calcite oxygen isotope composition ($\delta^{18}O_c$) and records detailed paleoclimatic information from the Late Miocene to the Early Pleistocene (9.8-1.8 Ma). Evidence is found for orbital forcing in the regional paleoclimate, with minimum and maximum eccentricity related to drier and wetter conditions respectively. Superimposed onto this variability, the long-term trend reflects the influence of global paleogeographic and climate change. Variations inferred in precipitation-evaporation (P–E) are related to SST in the North Atlantic, which evidences a connection between marine dynamics and continental climate in areas far from the coast in southwestern Europe and a relation between dry periods and high SST inland. It is proposed that the regional climate was impacted by the effect of the closure of the Central Atlantic Seaway and changes in the Atlantic Meridional Overturning Circulation (AMOC). Warmer/drier conditions were related to a more permanent, stable, high-pressure centre over the mid-Atlantic in a situation of strengthened AMOC, which would have blocked westerly winds, increasing aridity in southwestern Europe. The inferred warm/dry connection differs from other western Mediterranean records, supporting previous interpretations of a regional climate gradient in western Europe. As occurs at

present, isolation from the influence of the humidity of the Mediterranean Sea during warm periods as a result of' to the local orography could well have been the cause of regional differences.

Keywords

Paleoclimate, Lacustrine record, AMOC, Stable isotopes, Late Neogene, SW Europe

1. Introduction

After the Miocene Climatic Optimum (17-14.5 Ma), the global climate underwent a general cooling trend during the Late Miocene - Early Pleistocene, which resulted in a global temperature decrease of the order of 5-6°C (e.g. Utescher *et al.*, 2000; Zachos *et al.*, 2001; Lear et *al.*, 2003; Lisiecki & Raymo, 2005; Mosbrugger *et al.*, 2005; Bruch *et al.*, 2011; Quan *et al*., 2014; Holbourn *et al.*, 2018). Deep geological and paleogeographic changes during the Late Neogene reconfigured the climate system (e.g. Utescher *et al.*, 2000; Zachos *et al.*, 2001), and the climate zones came close to reaching the current setup. The main changes include the rise of mountain ranges (the Himalayas, Carpathians, Alps, Pyrenees, etc.), a new configuration of seaways and ocean circulation system, the appearance of the Sahara Desert, and the establishment of a permanent ice cap in the northern hemisphere (e.g. Ehleringer & Monson, 1993; Haug *et al.*, 2001; Griffin, 2002; Tuenter, 2004; Wang *et al.*, 2006; Potter & Szatmari, 2009; Dowsett *et al.*, 2009; Haywood *et al.*, 2009, 2016; Athanasiou *et al.*, 2015; Jiménez-Moreno *et al.*, 2018). Overlapping the long-term cooling, shorter-scale changes also occurred, whose local effects are less well known, especially in continental areas in which long and well-dated climate records are still lacking (e.g. Ditlevsen & Ashwin, 2018). At mid-latitudes, heat and moisture transport by ocean winds impacted on the continental rainfall and temperature (e.g. Bruch *et al*., 2011; Quan *et al*., 2014), but regional climates did not respond in a similar way to global changes, and climate variability and gradients between regions have been brought to light (e.g. Suc, 1978; Fauquette *et al*., 1999; Hernández-Fernández *et al*., 2007; Matson & Fox, 2010; Prista *et al*., 2015). The response of continental ecosystems differs depending on their latitude, continentality, altitude, and landscape (e.g. Fauquette *et al*., 2006; Bohme *et al*., 2011; Ribera d'Alcalà, 2019). In light of the foregoing, detailed continental paleoclimate reconstructions in diverse settings are key to understanding the variability and gradients within continents (e.g. Utescher *et al.*, 2012; Grygar *et al.*, 2017), as well as the factors forcing the changes.

Global circulation models of the Earth's changing climate agree that, with increasing temperatures in the future, a decline in precipitation is expected in Mediterranean areas as a result of the decline in the winter precipitation, in contrast with other regions in the world, where increasing precipitation is projected (Tuel & Eltair, 2020). The Western Mediterranean reached its present paleogeographic configuration during the Miocene, so deciphering Miocene-Pleistocene climate changes on multiple time scales and reconstructing the regional climate forcing, internal variability, and system feedback is paramount to understanding both past and future scenarios (Meyers *et al*., 2010). Although some studies have provided information on how terrestrial environments have reacted to long- and short-term climatic changes in the Western Mediterranean area (Suc, 1984; Bertini, 2001; Combourieu-Nebout *et al*., 2004; Jiménez-Moreno *et al*., 2010, 2013; De Miguel *et al*., 2018), more studies are still needed, including well-dated and calibrated proxy records in different geological/geographical settings (Ambar & Scarascia-Mugnozza, 2012).

Many continental proxies based on fauna, flora, or sedimentary features have proven very useful for paleoclimate studies (e.g. Fauquette *et al*., 1998, 1999; van Dam & Weltje, 1999; Utescher *et al.*, 2000; Teranes & McKenzie, 2001; Leng & Marshall, 2004; Mosbrugger *et al.*, 2005; van Dam, 2006; van Dam *et al.*, 2006; Domingo *et al.*, 2009; Barrón *et al.*, 2010; Domingo *et al.*, 2013; Suc *et al*., 2021). Paleontological data provide outstanding information but are sometimes lacking in resolution due to the inherent characteristics of the fossil record. Sedimentological, physical, and chemical proxies provide more continuous records (e.g. Quade *et al.*, 2007; Abels *et al*., 2009a,b; Pla-Pueyo *et al.*, 2015; Grygar *et al.*, 2017; Oliva-Urcía & Moreno, 2019). Among these, oxygen isotope values ($\delta^{18}O$) in lacustrine carbonates are widely used (e.g. Andrews *et al*., 2000; Teranes & McKenzie, 2001; Leng & Marshall, 2004; Luzón *et al*., 2009). Moreover, lacustrine basins potentially contain the most continuous and highest-resolution terrestrial records (see Fortelius *et al*., 2006).

The Teruel Basin (NE Iberian Peninsula), situated in a region of transition between Atlantic and Mediterranean influence, is a key area for the study of the Neogene continental climate in southwestern Europe. It records continuous deposition in a closed lake dating from 9.8 to 1.8 Ma and houses a huge amount of paleontological and magnetostratigraphic information, being a reference area for European Neogene mammal paleontology (e.g. Lindsay *et al.*, 1989). This basin is located in an intramountainous area with a significant orographic barrier to the east (Fig 1), and its current paleogeographic configuration was attained in the Late Miocene. As occurs at present, this situation would have isolated the study area from the influence of high Mediterranean Sea humidity. This work presents a new lacustrine calcite oxygen isotope record ($\delta^{18}O_c$) from this basin. As far as we know, it is the longest and highest-resolution continental climate curve of the Late Neogene in the Iberian Peninsula. Our main objectives are to decipher the climate signal recorded in the isotope data at different time-scales and interpret the principal triggers of the relevant changes, in order to provide new insights into the evolution of the climate and the variability of the western Mediterranean during the Late Miocene-Early Pleistocene. The $\delta^{18}O_c$ series records the most relevant climate changes described on a global scale and, from the Late Tortonian, shows a reasonable correlation with the sea surface temperatures (SST) in the North Atlantic. A warm/dry connection is inferred that differs from other western Mediterranean records, supporting previous interpretations of a regional climate gradient in western Europe (Suc, 1978; Fauquette *et al*., 1999; Matson & Fox, 2010; Prista *et al*., 2015; Jiménez-Moreno *et al*., 2009). Changes in the Atlantic Meridional Overturning Circulation (AMOC), superimposed orbital cyclicity (with eccentricity minima being related to drier conditions), and landscape barriers are suggested as triggers for the recorded paleoclimate changes.

2. Study area

The Neogene Teruel Basin is an elongated intramountain graben with an NNE-SSW trend (mean altitude: 989 m a.s.l.), located in the central-eastern Iberian Range, NE Iberian Peninsula (Álvaro *et al.*, 1979) (Fig. 1). The Iberian Range was formed as a result of the oblique collision between the Iberian microplate and the European plate from the Late Cretaceous to the Early Miocene (Álvaro *et al.*, 1979; Capote *et al.*, 2002). From the Middle Miocene, the central-eastern part of the mountain range was affected by extensional tectonics associated with the evolution of the Valencia Trough (Mediterranean Sea). As a result, the Iberian Range was cut obliquely by a series of extensional basins such as the Teruel Basin, which made it possible to accommodate a fairly continuous sedimentary infill (Simón, 1986; Capote *et al.*, 2002).

The Neogene Teruel Basin covers an area of 735 km^2 and is divided into two large sectors, the northern and southern sectors, which show differences in the structure and age of formation. The northern sector is the focus of this work (Fig. 2a), corresponding to a half-graben basin with an active N-S segmented margin at the eastern boundary (Ezquerro *et al*., 2020). It hosts an endorheic sedimentary succession spanning from the Late Miocene (~11.2 Ma) to the Early Pleistocene (~1.8 Ma) (Moissenet, 1983; Simón *et al*., 2012; Ezquerro *et al*., 2016, 2020). The estimated age is based on a large number of mammalian sites (e.g. Mein *et al.*, 1990; Alcalá *et al.*, 2000), as well as on magnetostratigraphic data (e.g. Krijgsman *et al.*, 1996; Opdyke *et al.*, 1997; Ezquerro *et al*., 2016) that yield a good chronological control related to Neogene continental mammal zones (MN zones; Mein, 1975), the European Land Mammal Ages (ELMA, e.g. Lindsay *et al.*, 1989), and the Geomagnetic Polarity Time Scale (GPTS; Ogg, 2012).

The vertical throw associated with the faults is 700 m, but the endorheic infill is less than 500 m thick, since the basin was captured by an external fluvial drainage around 1.8 Ma, when it evolved to exorheic conditions (Weerd, 1976; Moissenet, 1980; Godoy *et al.*, 1983; Ezquerro *et al.*, 2012, 2016; Ezquerro, 2017). During the Mio-Pleistocene, large and small alluvial fans, located at the passive and active basin margins respectively, graded to palustrine and lacustrine environments towards the central areas (Godoy *et al.*, 1983a,b; Moissenet, 1983; Alonso-Zarza *et al.*, 2000; Ezquerro *et al.*, 2014, 2019; Ezquerro, 2017). Thus, the endorheic infill comprises coarse-grained terrigenous facies close to the boundaries, corresponding to proximal sectors of alluvial fans, passing basinwards to medium and fine-grained detrital facies with local developments of calcretes, related to middle and distal areas of the alluvial fans. The distal alluvial facies grade to carbonates and minor gypsum, generated in shallow lacustrine-palustrine environments in the central part of the basin (Fig. 2b). The sedimentological features indicate that a closed, shallow lake existed in the Teruel Basin during the Mio-Pliocene, covering approximately 360 km^2 during stages of maximum expansion (Ezquerro *et al.*, 2014; Ezquerro, 2017). The overall lacustrine succession is represented by 209 m in thickness of carbonate deposits in the central areas of the basin, becoming thinner and disappearing towards the passive margin.

The sedimentary evolution was controlled by extensional tectonics (Ezquerro *et al*., 2014; Ezquerro, 2017; Liesa *et al.*, 2019). The propagation of faults at the basin margin controlled changes in sediment supply, as well as the distribution and evolution of the sedimentary systems. Angular unconformities, growth strata, and other evidence of active tectonism (e.g. seismites) have been found in relation to episodes of alluvial fan progradation and lake retraction (Ezquerro, 2017; Ezquerro *et al.*, 2019, 2020). In stages of decreasing tectonism, the alluvial fans retrograded, and the lake expanded, especially towards the passive margin. Climate also exerted notable control over sedimentation at different scales, and several climate-induced lake expansions/retractions have been inferred (Alonso-Zarza *et al.*, 2012; Ezquerro, 2017; Ezquerro *et al.*, 2014, 2019).

3. Methods

3.1. Sampling methods

The study record corresponds to a 212-m-thick composite lacustrine section that represents carbonate sedimentation in the Neogene lacustrine system of the Teruel Basin (Fig. 3). The sampled succession is based on the correlation of three stratigraphic profiles (selected for the isotope study due to their high carbonate content), in turn based on well-dated guide levels or packages, identifiable by particular lithological or sedimentological characteristics. The sampling protocol focused on obtaining nearly constantly spaced (one sample per metre), unaltered samples of the lacustrine succession, resulting in a total of 202 samples. The sampling density allowed an accurate correlation between different outcrops, avoiding large data gaps. In each profile, all the samples were located in their precise stratigraphic position at decimetre precision. Rock blocks were collected using hammers and chisels in the field to obtain a significant volume of sample (cm-scale) for performing thin sections as well as mineralogical and geochemical analyses. The subsequent laboratory procedures were based on extracting small cores from the blocks, which avoids alterations or disturbances from the surrounding materials. The cores were extracted with an electric drill and a hollow drill bit made of stainless steel with a diamond head or, when this was not possible, with rotary saws.

3.2. XRD mineralogical analyses

The mineralogy of the lacustrine carbonates was determined using RIGAKU D/max2500 and Philips PW 1729 diffractometers from the X-ray Diffraction and Fluorescence Analysis Service (Research Support Services) and the Earth Sciences Department, respectively, in the University of Zaragoza. The configuration of the diffractometers was 40Kv and 80 mA with Cu anodes and a graphite monochromator to select the Cu K-alpha radiation. The analyses were carried out on powdered samples, crushed manually by an agate mill, and sieved at 53 μm. The measurement conditions were established at room temperature with 2θ angles from 3º to 60º and steps of 0.04º and 0.4 s/step. The resulting diffractograms were interpreted by the XPowder 12 software using the fundamentals of reference intensity (RIR; Chung, 1974) and the Rietveld method (Rietveld, 1969).

3.3. Microtextural analyses: FESEM and optical microscopy

Selected samples were analysed by field emission scanning electron microscopy (FESEM) using secondary (SE) and backscattered electron (BSE) images and energy-dispersive X-ray (EDS) analysis. The observations were performed using a Carl Zeiss MERLIN FESEM equipped with an Oxford Instruments INCA 350 EDS detector of the Research Support Services of the University of Zaragoza. Elemental analyses were made with an accelerating voltage of 133 eV to 5.9 KeV and a beam current of 80 nA. Samples were gold-coated. Photomicrographs were taken in imaging mode with secondary electrons. Petrographic observations were made by optical microscopy using conventional thin sections made at the Research Support Services of the University of Zaragoza.

3.4. Stable isotope analyses ($\delta^{18}O$ and $\delta^{13}C$)

The selection of samples was based on mineralogical X-ray and petrographic results in order to avoid non-primary carbonates. Only samples with authigenic calcite and without dolomite or other carbonate minerals were considered. With a view to avoiding any influence from non-authigenic calcite sources, samples with appreciable fossil content or carbonate extraclasts were not selected. Likewise, samples with low percentages of calcite were discarded. Isotope analyses were performed on calcite samples acquired on whole sample by grinding an agate mill and sieving at 53 μm. In each sample, 10 to 15 mg of rock powder was used and treated with 1 ml of 103% H_3PO_4. The CO_2 was extracted following the techniques described by Walters *et al.* (1972), and each of the fractionated extractions was treated with Ag_3PO_4 to eliminate the possible SO_2 released. Sampling and analyses were carried out at the Stable Isotope Laboratory of the University of Salamanca, using a dual inlet SIRA-II mass spectrometer. The measurements were made under vacuum conditions (McCrea, 1950), with a temperature of 25ºC in the carbonate line and 90ºC with the IsoCaRB system. The precision of the method is 0.2‰ for $\delta^{18}O$ and 0.1‰ for $\delta^{13}C$. The obtained results are presented in relation to the international VPDB standard (Craig, 1957; Gonfiantini, 1984).

3.5. Spectral and cyclicity analyses (depth domain)

The spectral and cyclostratigraphic analyses were developed in a continuous quantitative time series of 118 data corresponding to the $\delta^{18}O$ values of the lacustrine calcite ($\delta^{18}O_c$). Before performing the spectral analysis, taking into account the different sampling intervals, an interpolation of the time series (every 1 m) was performed using the software Acycle v2.1 (Li *et al.*, 2019). The methodology also includes trend elimination (with the LOESS model; Cleveland, 1979) and spectral analysis (depth domain) using the Multi-Taper method (MTM; Thomson, 1982). With the aim of characterizing the lower-frequency cycles, the time series was smoothed with a Gaussian filter. The anchoring between the cycles resulting from the spectral analysis and the Milankovitch cycles was performed using the Correlation Coefficient tool (COCO and eCOCO) of the Acycle v2.1 software, which provides the most probable value for the sedimentation rate; the anchor allows thickness cycles (depth domain) to pass into time cycles (time domain).

4. Results

4.1. Sedimentological features

The sedimentary succession is mainly formed by limestones, marls, carbonate silts, and nodular carbonates, with some intercalations of mudstones, gypsums, and sandstones towards the upper part (Fig. 3). Greyish to whitish limestones, in tabular or irregular strata, predominate in the lower and middle part of the succession, exhibiting two main facies: massive mudstone-wackestone and bioturbated wackestone-packstone (Fig. 4); laminated facies are recognized only occasionally. Bioturbated facies show vertical root traces and brecciation. Charophytes and gastropods are the most common fossils in both kinds of facies, which rarely show intraclasts. Massive limestones represent lacustrine inner or sublittoral facies, whereas bioturbated limestones indicate littoral to palustrine conditions. Greyish to greenish marls show a massive, rarely laminated texture and contain charophytes, gastropods, and plant debris. They usually appear as tabular or irregular layers between limestones and carbonate silts. Whitish carbonate silts are more common in the middle-upper part of the succession and form massive or laminated tabular beds with occasional gastropods and plant remains (Fig. 3). Marls and silts represent the entry of water and terrigenous supplies into the lake. On the basis of these features, sedimentation in a wide, shallow, low-energy carbonate lake has been inferred (Alonso-Zarza *et al.*, 2000, 2012; Ezquerro *et al.*, 2014; Ezquerro, 2017).

According to the optical microscopy and scanning electron microscopy (FESEM) observations, the mineralogical data indicate an authigenic origin for the calcite (Cc), since no textural evidence of diagenetic calcite replacement is observed (Fig. 5). Calcite forms small euhedral-subhedral crystals with knobby surfaces. Calcite and quartz (Qz) + phyllosilicates (Phy) show a negative correlation (R = - 0.58; 202 samples) (Fig. 6a), indicating that they were favoured under different sedimentary conditions. On the other hand, quartz and phyllosilicates show a positive correlation, which is indicative of a common origin related to detrital input (Fig. 6b). A very high negative correlation emerges when (Qz + Phy)/ (Cc + Gy) are compared (R = - 1), indicating a non-genetic relation between the two sets (Fig. 6c). Moreover, gypsum (Gy) and calcite (Cc) show a strong negative correlation (R = - 0.76), which suggests non-simultaneous precipitation (Fig. 6d), with gypsum precipitation being favoured in more concentrated waters.

4.2. The $\delta^{18}O_c$ lacustrine record

The calcite $\delta^{18}O_c$ curve is based on detailed sampling and analysis of 202 lacustrine carbonate samples (approximately one per metre). In the end, however, 182 samples were included in the composite record due to the overlapping of 20 samples between correlated profiles. The isotopic signal of the overlapping samples is reproducible and replicable in the sense of Mangini *et al.* (2007) or Dorale & Liu (2009), which reinforces the hypothesis of a precipitation of carbonates in equilibrium with lake waters. The different $\delta^{18}O_c$ values of the Mesozoic rocks in the source area (Luzón *et al.*, 2009; Colás *et al.*, 2010; Val *et al.*, 2017) rule out a significant influence of detrital carbonates on the isotopic signal (Fig. 7). The positive correlation between the $\delta^{18}O_c$ and $\delta^{13}C_c$ values indicates closed lacustrine hydrological conditions (Fig. 7), the influence of the air-water exchange being reflected in the isotopic signal (Talbot, 1990; Li & Ku, 1997; Valero-Garcés *et al.*, 1997; Ezquerro *et al.*, 2014).

The $\delta^{18}O_c$ values are always negative and range between approximately –2‰ and –10‰, with an average (χ) of –5.8 ‰ and a standard deviation (σ) of 1.3 ‰ (Fig. 3). Despite the significant variability of the $\delta^{18}O_c$ values, three main periods in the order of

10^6 years can be recognized by comparing the $\delta^{18}O_c$ trend with the average value (Fig. 3). The oxygen isotope data also reveal high climate variability, especially for Periods 2 and 3.

Period 1 comprises 40 data with values between –5.0 ‰ and –7.4 ‰ and covers from the Middle to the Upper Tortonian (~9.8 to ~8.6 Ma). This part of the succession is characterized by lower $\delta^{18}O_c$ values than the average, with χ = –6.3 ‰ and σ = 0.5 ‰ (Fig. 3). Low $\delta^{18}O_c$ intra-variation exists, with a slight increase towards the upper part of the period (Fig. 3). Previous studies have shown that during this period the lake system showed a high width/depth ratio in the initial phases of basin development (Ezquerro *et al.*, 2014, 2020; Ezquerro, 2017).

Period 2 includes 67 samples that represent the Late Tortonian-Late Zanclean interval (~8.6 to ~3.6 Ma). The data range from –6.8 ‰ to –2.3 ‰, with χ = –4.8 ‰ and σ = 1.0 ‰, and with a higher $\delta^{18}O_c$ mean value in this period than in the succession as a whole and notably higher than the average for Period 1 (Fig. 3). The $\delta^{18}O_c$ variability increases with respect to Period 1, and most values exceed the average. Higher values are found in three intervals over the course of this period: from ~8.5 to ~8.1 Ma, ~6.0 to ~5.7 Ma, and ~5.1 to ~4.2 Ma; the latter interval shows the highest values for the whole time span under study. Some intervals (~7.1 to ~6.6 Ma; ~6.1 to ~6.0 Ma, ~5.3 to ~5.1 Ma) and several excursions (e.g. taking place between ~4.8 and ~4.0 Ma) with values below the basin average can also be recognized. As a consequence, the series of $\delta^{18}O_c$ values is highly oscillatory, especially from the middle-upper part of Period 2, with variations sometimes of up to ~4.0 ‰. In Period 2, two main lake expansions were recorded, with maxima around 6.9 Ma and 4.4 Ma. These were separated by a phase of lacustrine retraction around 6.0 Ma (Ezquerro *et al.*, 2014, 2020; Ezquerro, 2017). Facies analysis indicates that shallow lacustrine conditions always prevailed.

Period 3 is defined by 75 data covering Piacenzian and Early Gelasian stages (from ~3.6 to ~1.8 Ma). In contrast to Period 2, $\delta^{18}O_c$ values are lower than the basin average, especially in the lower part (Fig. 3), ranging from –9.8 ‰ to –3.5 ‰ (χ = –6.5 ‰ and σ = 1.3 ‰). The intra-period variation is high, and values oscillate very quickly (changes of up to ~4.5 ‰) but are only higher than the basin average around 3.1-3.2 Ma and between ~2.9 and ~2.5 Ma. From 2.2 Ma to more modern times, the values are close to the basin average, and very few excursions are recognized. During this period, the lake system became more restricted and shallower due to the segmentation of the basin and isolation of several depocentres in consequence of fault activity (Ezquerro *et al.*, 2014, 2020; Ezquerro, 2017).

4.3. Spectral analysis of the $\delta^{18}O_c$ time series

In order to recognize an external forcing superimposed upon the tectonics, the cyclicity analysis was based on the $\delta^{18}O_c$ values and their correlation with the thickness of the sedimentary succession. Previous works (Krijgsman *et al.*, 1996; Garcés *et al.*, 1999) have suggested the existence of a hiatus around the Middle Turolian (Tortonian – Messinian boundary), between chrons C4n.1r and C3Ar, but the absolute dating has remained unresolved. Recently, Ezquerro (2017) and Ezquerro *et al*. (*submitted*), integrating information from the stratigraphic framework, mammal sites, and the magnetostratigraphic context, have shown that the proposed hiatus coincides with an interval with a very low sedimentation rate between ~7.9 and ~6.6 Ma. In our stratigraphic succession, this interval occurs in the middle part and is poorly defined, with seven samples representing a period of around one million years. Taking this into consideration, and in order to avoid any disturbance related to the existence of a hiatus or a period of very low sedimentation, the spectral analysis focused on the 6.15 to 1.8 Ma interval (66-209 m).

The spectral analysis was performed over 143 metres that correspond to 118 data, with an average sampling interval of 1.2 m (interpolated to 1 m for the spectral analysis). Bearing in mind that to define a cycle at least two data are needed (Nyquist frequency), the thinnest cycle that could be recognized would be 2 m thick. As according to the spectral analysis results (depth domain, Fig. 8), the thickness of the obliquity and precession cycles should be 1.9 and 0.95 m, respectively, it was not possible to discriminate them with the available sampling density. Two cycles (13.33 m and 4.77 m) exceed the 99.9% confidence band (Fig. 8b). Given the resulting average sedimentation rate of 3.61 cm/ka for the interval between 66 and 209 m of the $\delta^{18}O_c$ time series (Fig. 9), these cycles lasted 369 ka and 132 ka, respectively. However, the sedimentation rate analysis undertaken with the Acycle-eCOCO software (Li *et al.*, 2019) indicates noticeable changes throughout the series, although the rate remained very constant between 3.1 and 1.8 Ma (140 and 209 m, respectively; Fig. 9). The spectral analysis of this part of the succession suggests that the two maxima above the 99.9% confidence band correspond to cycles of 14.58 m and 4.32 m (Fig. 8c). Based on the inferred average sedimentation rate (3.61 cm/ka), the cycles span ca. 404 ka and 120 ka, respectively, which is very close to the two eccentricity modes (< 10% error).

After applying a Gaussian filter (interpolated every metre and removing the trend with a LOESS model), with the filter centre at 405 ka and 2.4 Ma, the anchoring of the filtered $\delta^{18}O_c$ time series to the La2010a solution (Laskar *et al.*, 2011) was performed using the paleontological and magnetostratigraphic data for the Teruel Basin (e.g. Mein *et al.*, 1990; Krijgsman *et al.*, 1996; Opdyke *et al.*, 1997; Ezquerro, 2017) in order to introduce the time coordinate (Fig. 8d). The $\delta^{18}O_c$ oscillations of the filtered curve match the eccentricity component of the orbital forcing, with the maximum and minimum eccentricity values being correlated, respectively, with the lowest and highest $\delta^{18}O_c$ values.

5. Discussion

5.1. On the origin of the $\delta^{18}O_c$ signal

The isotopic composition of lacustrine authigenic carbonates is directly related to the temperature and $\delta^{18}O$ of the lake waters ($\delta^{18}O_w$) (e.g. Leng & Marshall, 2004; Hoefs, 2009). In open lakes with a short residence time, the $\delta^{18}O_c$ values reflect seasonality, temperature, and the rainfall water $\delta^{18}O$ composition. By contrast, closed shallow lakes are more sensitive to long-term changes in the P–E rate due to the long residence time of the water (Li & Ku, 1997; Andrews *et al.*, 2000; Leng & Marshall, 2004). In closed and shallow lacustrine systems, the P–E ratio, controlled by temperature and humidity conditions, thus has a greater impact on the isotopic composition of the lake water compared to other factors such as changes in the source of moisture. However, more complex relationships are possible, since the factors that control basin hydrology can interact with each other (e.g. Jones & Roberts, 2008; Benavente *et al.*, 2019). In order to shed light on the climate signal recorded in the $\delta^{18}O_c$ in the Neogene Teruel Basin, the climate factors that controlled the isotopic composition of the lacustrine calcite are here discussed.

As explained above, the sedimentological data support a large palustrine-shallow lacustrine area dominated by closed hydrological conditions during the Late Neogene-Early Pleistocene. The $\delta^{18}O_c$ values generally lie within the range of freshwater lakes, and the positive $\delta^{18}O_c$ / $\delta^{13}C_c$ covariance agrees with the closed hydrological conditions inferred (Talbot, 1990; Li & Ku, 1997; Leng & Marshall, 2004). By the same token, the high $\delta^{18}O_c$ variability is not consistent with an open lake in which the water composition is mainly homogeneous (e.g. Valero-Garcés *et al.*, 1997; Jones & Roberts, 2008), leading to low isotope variation (Quade *et al.*, 1995; Dunagan & Turner, 2004; Luzón *et al.*, 2017). Only the low variation in $\delta^{18}O_c$ recorded in Period 1 could indicate damping processes, which Ezquerro *et al.* (2014) relate to fault activity. Whatever the case, as suggested by Talbot (1990), these isotopic features are typical of lakes with a low width/depth ratio, which is consistent with the sedimentological interpretation for Period 1. The $\delta^{18}O_c$ / $\delta^{13}C_c$ covariance, the generally high $\delta^{18}O_c$ variability, and the amplitude of the range values point to the P–E ratio as the direct control factor for the calcite isotope values. Several studies point out that, in palustrine areas and shallow lakes, the influence of temperature through surface evaporation on isotope composition is greater than groundwater (e.g. Jones & Roberts, 2008; Benavente *et al.*, 2019).

In summary, it is proposed that the calcite isotope values in the Late Neogene Teruel Basin would have been controlled by changes in humidity but also in temperature. With higher temperatures, relatively $\delta^{18}O$-enriched precipitation and increasing lake water evaporation (with preferential ^{16}O loss) would have led to a rise in the $\delta^{18}O$ of the lake water and in the precipitated carbonates. Therefore, higher $\delta^{18}O_c$ values would record drier (a lower P–E ratio) and warmer periods. Conversely, lower $\delta^{18}O_c$ values may be related to lower temperatures, which would have favoured isotopically depleted rain (Craig, 1961) and reduced evaporation (a higher P–E ratio) in the lake.

Comparisons between our data and previous results providing mean annual temperatures (MAT) and mean annual precipitation (MAP) based on the $\delta^{18}O$ signature of mammal dentition (van Dam & Reichart, 2009; Matson & Fox, 2010; Domingo *et al.*, 2009, 2013) or micromammal associations (van Dam & Weltje, 1999; van Dam, 2006; van Dam *et al.*, 2006) reinforce this interpretation (Fig. 10), since the curves proposed for these authors show very similar trends to that of our $\delta^{18}O_c$. The $\delta^{18}O$ isotope data from large-mammal tooth enamel (van Dam & Reichart, 2009; Matson & Fox, 2010; Domingo *et al.*, 2009, 2013) present lower resolution than the small-mammal records but are also key to relating temperature and humidity conditions. The range and position of the $\delta^{18}O_c$ variations in the Teruel Basin are comparable to the macromammal data, which also support the influence of temperature. The $\delta^{18}O$ variations recorded in the dentition were interpreted as changes in temperature between 11.1 °C and 23.8 °C (van Dam & Reichart, 2009; Matson & Fox, 2010), and, with minor variations, they show a general decrease in temperature (5 to 6°C) over the course of the study period (e.g. van Dam & Reichart, 2009; Domingo *et al*., 2013; De Miguel *et al*., 2019).

The connection between the warmer/drier stages is also in line with climate interpretations for the Teruel Basin and other Iberian records (Daams *et al*., 1988; van Dam and Weltje, 1999; Hernández-Fernández *et al*., 2007; Domingo *et al*., 2009, 2013; van Dam & Reichart, 2009; Matson & Fox, 2010; De Miguel *et al*., 2018). Nevertheless, in Mediterranean coastal zones, a connection between warming and more humid stages has been proposed, as well as a latitudinal temperature and precipitation gradient between northern and southern areas since the Middle Miocene (Suc, 1978; Fauquette *et al*., 1999; García Alix *et al*., 2008; Matson & Fox, 2010; Suc *et al*., 2018; Jiménez Moreno *et al*., 2019). Accordingly, in the Iberian area when the climate was warmer and more humid in the northern Mediterranean, warmer and drier conditions prevailed in the southern Mediterranean. At present, the climate of the Iberian Peninsula features marked regional and seasonal variability, which is the result of the interaction of different air masses with a complicated orography and is strongly influenced by the surrounding water masses (Cabos *et al*., 2020). Regional differences in the Late Neogene would have been associated, as at present, with the orographic barriers in the S-SE (in this case the Iberian Range), preventing a high Mediterranean oceanic influence. Currently, vegetation models for the Mediterranean based on pollen records show a zonal distribution through the Iberian Peninsula (Favre *et al*., 2007; Jiménez-Moreno *et al*., 2010), with a clear limit (xerophytic vegetation/subtropical forests) near the Teruel Basin. The presence of such a limit agrees with the occurrence of the particular environmental conditions for this intramountainous basin during the Late Miocene (which more general climate models fail to establish).

5.2. Climate changes inferred from $\delta^{18}O_c$ *and correlation with other climate records*

The isotope curve of the Teruel Basin records short and long-term climate changes and three periods with very distinct climate conditions. The general cooling trend documented worldwide after the MCO (Miller *et al*., 1991; Zachos *et al*., 2001; van Dam & Reichart, 2009; Super *et al*., 2020) is recorded by a general decrease in $\delta^{18}O_c$ values from Period 1 to 3. The range of the $\delta^{18}O_c$ changes (in average values) recorded in the

Teruel lacustrine carbonates could represent an extreme increase of ~6°C between Periods 1 and 2, and a decrease of ~7ºC between Periods 2 and 3 (Fig. 10). It should be noted that in comparison with previous records, our $\delta^{18}O_c$ curve additionally shows high-frequency climate variability in the Teruel Basin, considerably improving the resolution of climate information for this Iberian area.

Broadly, Period 1 (~9.8 to ~8.6 Ma) was relatively humid (high P–E) and cool, as inferred from the lower $\delta^{18}O_c$ values (average -6.4‰) with respect to the mean. Furthermore, a low standard deviation for $\delta^{18}O_c$ suggests low climate variability. Such conditions in the Teruel Basin correlate well with a stage of relative global cooling, which has been associated with lower levels of atmospheric pCO_2 (see Fig. 11; Pearson & Palmer, 2000; Pagani *et al*., 2010; Seki *et al.*, 2010; Stap *et al.*, 2016) and the arrival of ice-rafted debris at low latitudes (Thiede *et al.*, 1998; Winkler *et al.*, 2002) during this time. The models of mean annual precipitation (MAP) for the Teruel Basin, based on changes in the arboreal and invertivore mammal communities, also indicate wetter-cooler conditions until ~8.6 Ma. Other pollen and micromammal proxies point to an increase in precipitation in Europe, with (sub)humid climatic conditions prevailing during this period (van Dam, 2006; Donders *et al*., 2009; Utescher *et al.*, 2012; Quan *et al*., 2014). Nevertheless, some authors propose warm and humid conditions in southwestern and central Europe (Böhme *et al.*, 2008). Low climate variability during the Late Tortonian has also been evidenced in ocean records (Herbert *et al*., 2016; Super *et al*., 2020), as well as in other continental proxies such as pollen records from the south of the Iberian Peninsula (Postigo-Mijarra *et al.*, 2009). This could be related to the fact that a Mediterranean-type climate, dry in summer, had not yet been established (Quan *et al*., 2014).

A noticeable increase in $\delta^{18}O_c$ values (average ~2‰) at ~8.6 Ma characterizes the transition to Period 2 (~8.6 to ~3.6 Ma) and testifies to a net decrease in the P–E ratio and increasing temperatures in the Teruel Basin (Figs. 10 & 11). Such a change coincides with a general increase in pCO_2 (e.g. Pagani *et al.*, 2005) and an increase in SST (~5ºC) at mid-latitudes (Herbert *et al.*, 2016 and references therein), as well as with the expansion of C4 plants (Cerling *et al*., 1997; Edwards *et al.*, 2010) on a global scale. A wet–dry seasonal climate has been interpreted for the Teruel Basin until ~8 Ma (van Dam & Weltje, 1999), although a faster decrease in the winter rainfall than in the MAP suggests increasing aridification around 8.5 Ma, when the establishment of a dry season was definitive and higher mean temperatures were reached during the colder months (van Dam, 2006). The disappearance of many paleotropical taxa and aquatic plants in the Iberian Peninsula (Böhme *et al.*, 2008; Postigo-Mijarra *et al.*, 2009) and faunal changes (e.g. Blanco *et al.*, 2018; De Miguel *et al.*, 2019) also indicate warmer conditions, which in turn suggest more effective evaporation than precipitation (Fig. 10). However, in the Granada and Crevillente basins (SE Spain), the climate in the Latest Tortonian was temperate and more humid conditions than for the Teruel Basin have been deduced, evidencing regional differences in Iberia. At a global scale, the European Temperate Wet Zone (ETWZ) contracted from ~9 Ma onward, and the Subtropical High-Pressure Zone (SHPZ) expanded, as southern and western Europe and eastern Asia evolved towards drier conditions (Haug *et al.*, 2001; Griffin, 2002; Barrón *et al.*, 2010; Böhme *et al.*, 2008, 2011).

After the increase in SST at ~9 Ma, a general cooling trend characterized the Late Miocene (Miller *et al.*, 1991; Zachos *et al.*, 2001; Herbert *et al.*, 2016; Super *et al.*, 2020). By contrast, warm conditions, low P–E rates, and increasing climate variability are deduced from our isotope curve for the Teruel Basin between the Late Tortonian and the Zanclean (ca. 4.3 Ma). This trend changed towards the Piacenzian to a more humid and cooler climate (Period 3), with the record showing a clear shift towards lower $\delta^{18}O_c$ values; the lowest values are recorded from 3.6 to 3 Ma. The models of mean annual precipitation (MAP) for the Teruel Basin, based on changes in the arboreal and invertivore mammal communities, also indicate warmer/drier conditions from the Late Tortonian to the Zanclean, which correspond to increases in MAT of up to 7°C and evaporative enrichment during the summer (van Dam & Reichart, 2009; Matson & Fox, 2010). Although a generally warm climate is demonstrated for the Late Miocene-Early Pliocene, wetter-cooler conditions prevailed during some periods in the region, as indicated by several gentle excursions to lower $\delta^{18}O_c$ values (e.g. ~7.1 to 6.6 Ma, 6.1 to 6 Ma, ~5.3 to 5.1 Ma, and some other episodes in the Zanclean; Fig. 11). This agrees with previous interpretations (van Dam & Weltje, 1999; van Dam, 2006; van Dam *et al.*, 2006, 2009) proposing drops in the MAT due to the higher influence of the low winter temperatures and cooler summers (van Dam & Reichart, 2009; Matson & Fox, 2010).

Increasing temperature and warming conditions for the Late Miocene-Early Pliocene have also been inferred from fauna and vegetation in western European and Mediterranean regions (Fauquette *et al.*, 2007; Hernández-Fernández *et al.*, 2007), with severe aridity occurring in many regions (Fauquette *et al*., 1999; Barrón *et al*., 2010; Pellegrino *et al*., 2018; Suc *et al*., 2018; Jiménez Moreno *et al*., 2019), followed by a general temperature decrease (Fauquette *et al*., 2006). Our isotope curve suggests that although aridity intensified during the Messinian, no dramatic climate changes occurred during the Messinian Salinity Crisis (~5.9 to 5.3 Ma), as previously proposed for the Mediterranean coastal zone (Fauquette *et al*., 1999, 2006; Jiménez Moreno *et al*., 2009; Barrón *et al*., 2010). Between 5 and 4 Ma, aridification became more severe in the Teruel Basin, and wet-season precipitation decreased (van Dam & Weltje, 1999; van Dam, 2006; van Dam *et al.*, 2006, 2009); this is recorded by the higher $\delta^{18}O_c$ values in our record, which rarely fall as far as average levels.

The transition to Period 3 (~3.6 to ~1.8 Ma) is characterized by a sharp decrease in the $\delta^{18}O_c$ values (average: -6.4‰), the lowest values of the whole succession generally being recorded. The higher P–E ratio and lower temperatures in the Teruel Basin (Figs. 10 & 11) are consistent with the global climate cooling that occurred from the Mio-Pliocene boundary to the end of the Zanclean (Lisiecki & Raymo, 2005; Karas *et al*., 2017), which has been associated with the onset of northern hemisphere glaciation, with a temperature decrease in Europe and the growth of the Arctic ice sheet (e.g. De Schepper *et al.*, 2013). CO_2 concentrations decreased during the Piacenzian-Gelasian (Pearson & Palmer, 2000). Our curve also reflects a clear increase in climate variability, which chimes with the SST records (e.g. Lawrence *et al*., 2010; Herbert *et al*., 2016). Many shorter-term drier and warmer episodes (more positive $\delta^{18}O_c$) can be deduced in the Teruel record, such as the mid-Pliocene Warm Period (mPWP) between 3.2 and 3.0 Ma, as well as many other positive $\delta^{18}O_c$ excursions, which we propose, on the basis of their age, to be related to Marine Isotope Stages (Fig. 11). The identification of MIS effects in continental records has also been suggested by Suc *et al*. (2018). The driest conditions during this period were reached from 2.5 to 2.9 Ma, in accord with the results published by van Dam & Reichart (2009) and Rodríguez-López et al. (2012). As in previous periods, high $\delta^{18}O_c$ variability could correspond to an increase in MAP and related seasonal oscillations. The MAP estimates for the Teruel Basin are less well defined for the Late Pliocene (from ~2.6 Ma on), but a general increase in precipitation rates has been inferred, with high variations, as a consequence of glaciations (Fauquette *et al.*, 1998).

5.3. Triggers of the climate intra-variability: orbital forcing and the dynamics of the north Atlantic Ocean and Mediterranean Sea

The three long-term climate periods (1 to 3), as well as the shorter-term climate variations defined on the basis of $\delta^{18}O_c$ values, suggest that several superimposed factors controlled the environmental conditions in the eastern Iberian Peninsula. Here we discuss proposals, apart from orbital forcing, for how the north Atlantic Ocean and the Mediterranean Sea impacted on climate in the Neogene Teruel Basin.

As previously stated, the influence of astronomical forcing has been demonstrated by correlating the lowest isotopic values with maxima in eccentricity, and vice versa (Fig. 8). In addition, lower $\delta^{18}O_c$ values are associated with deeper sedimentary facies, indicating a relatively high water table. In light of the foregoing, wetter and cooler (low $\delta^{18}O_c$) episodes are correlated with eccentricity maxima, whereas warming episodes with enhanced evaporation (high $\delta^{18}O_c$) are correlated with eccentricity minima (Fig. 12). This interpretation is in line with that proposed by Abels *et al*. (2009a,b) based on the study of palustrine-lacustrine facies in the southern part of the Teruel Basin. These authors suggested a modulation of summer/winter insolation and winter precipitation through the influence of obliquity and precession. It is highly probable that lower-order orbital cycles influenced climate variability and shorter-term changes in our record, but the current sampling resolution precludes confirmation of this hypothesis.

Comparison of the Teruel $\delta^{18}O_c$ curve with oceanic records (Fig. 11) suggests that variations in the AMOC might have had a deep impact on changes in humidity and temperature in the inland areas of the eastern Iberian Peninsula; the magnitude and timing of these changes can be inferred from our $\delta^{18}O_c$ curve (Fig. 11). It is known that although orographic barriers may influence the circulation of air masses, ocean dynamics exerts direct control over mid-latitude continental areas, since the winds that transport heat and moisture landwards influence rainfall rates and temperature (Bruch *et al.*, 2011; Herold *et al.*, 2012; Quan *et al.*, 2014; Sherriff-Tadano *et al.*, 2018). The correlation between Mio-Pliocene terrestrial and marine climate records in Europe has been documented in many works. Mid to Late Miocene pollen records in northwestern Europe show a strong coupling between marine and terrestrial temperatures, although the cooling trend seems to have been more gradual in inland areas (Donders *et al*., 2008, 2009). During the Middle Miocene, central Europe was under oceanic influence, displaying a warm and wet climate very consistent with increases in global warming intervals and seasonality during cooling periods (Methner *et al.*, 2020). Around the Mediterranean Sea, vegetation and climate changes that occurred during the Pliocene are in good agreement with pollen records from NW Europe and $\delta^{18}O$ curves from Mediterranean and Atlantic deep-sea cores (Fauquette *et al*., 1999). The $\delta^{18}O_c$ record for the Teruel Basin also shows a similarity with North Atlantic marine records, especially from 8.6 Ma, and at a lower scale marine isotope stages (MIS) are reflected in the curve (Fig. 11).

Today, the Atlantic Ocean is the primary source for Iberian precipitation. Recent modelling work indicates that the precipitation gradient is controlled by the stronger Atlantic influence in the northern and eastern areas, especially during the winter season, with precipitation and temperatures being controlled by the air-ocean coupling (Cabos *et al*., 2020). Modern temperatures and rainfall $\delta^{18}O$ values in eastern Iberia also show a predominance of the Atlantic fronts, whereas the Mediterranean convective rainfalls have less impact and play a significant role especially in summer, when the influence of the large-scale Atlantic circulation is reduced (Moreno *et al.*, 2014, 2021; Pérez-Mejías *et al.*, 2018; Cabos *et al*., 2020). The present-day records in eastern Iberia also indicate a close relationship between Atlantic Ocean temperatures and relative humidity as the main drivers of the P–E rate, suggesting that $\delta^{18}O$ values in the continental realm are highly sensitive to these changes (e.g. Pérez-Mejías *et al.*, 2018). Inter-annual rainfall oscillations are controlled by the seasonal migration of the Subtropical High-Pressure Zone (SHPZ) and changes in the North Atlantic Oscillation (NAO) (Moreno *et al.*, 2014; Hernández *et al.*, 2015). As the main orographic barriers have not changed since the Late Miocene, it is thought that a similar situation must have prevailed in the Iberian Peninsula since then and that changes in temperature and moisture in the Atlantic have had a strong influence on inland areas.

A remarkable, dramatic transition in the oceanic and atmospheric circulation was associated with huge paleogeographic changes during the Late Neogene (Haug *et al.*, 2001; Zachos *et al.*, 2001; Quan *et al.*, 2014). During this period, global climate conditions changed until an Earth configuration similar to today's was reached. A shift in the atmospheric circulation in the Tortonian (Quan *et al.*, 2014), with a high-pressure system over Atlantic mid-latitudes, imposed the ocean-water and atmospheric pattern that currently prevails in western Europe, with dominant westerly winds in Europe (Quan *et al.*, 2014; Bell *et al.*, 2015; Herold *et al.*, 2012; Sherriff-Tadano *et al.*, 2018). Although the closure of the Central Atlantic Seaway (CAS) started ~15 Ma ago, the first emergence of land and the early disconnection between Pacific and Atlantic deep-waters occurred from ~10 to ~7 Ma, and the disconnection of surface waters took place between ~3.5 and 2.5 Ma (Molnar, 2008; Bell *et al.*, 2015). The Pacific-Atlantic disconnection triggered the intensification of the Atlantic Meridional Overturning Circulation (AMOC), and the transport of heat and moisture in the Atlantic became more efficient (Karas *et al.*, 2017), impacting the global atmospheric circulation and the climate in western Europe landwards (Böhme *et al.*, 2008; Bell *et al.*, 2015; Lohman *et al.*, 2015; Karas *et al.*, 2017). In general, since the closure of the CAS (~7 Ma), water exchange between the Pacific and Atlantic oceans has been severely restricted. Nevertheless, a temporary connection between the two oceans has been reestablished during some episodes, triggering AMOC weakness (Böhme *et al.*, 2008; De Schepper *et al.*, 2013). The strengthening or weakening of the AMOC implies, respectively, an increase or decrease in the SST in the North Atlantic, the changes at the mid-high latitudes of the northern hemisphere being more marked since the closure of the CAS (Molnar, 2008; Bell *et al.*, 2015). A general synchrony between the oscillations of the SST in the different North Atlantic Ocean Drilling Program (ODP) sites has been shown since the closure of the CAS (Molnar, 2008; Zhang *et al.*, 2013; Fedorov *et al.*, 2013; Bell *et al.*, 2015) (Fig. 11). In addition to the evolution of the CAS, changes in the Arctic gateways through the NADW (Bell *et al.*, 2015) and the Mediterranean outflow into the Atlantic waters (Pérez Asensio *et al.*, 2012; Ivanovic *et al.*, 2014) could have also impacted the strengthening or weakening of the AMOC during some episodes (Karas *et al.*, 2017).

As previously stated, until ~8.6 Ma our isotope record and the SST of the Atlantic Ocean show low variability (Fig. 11), a situation that could be associated with the incipient closure of the CAS and a possible water exchange between the Pacific and Atlantic Oceans that drove a weak North Atlantic circulation (Molnar, 2008; De Schepper *et al.*, 2013; Bell *et al.*, 2015). The still open oceanic connection could have induced anomalies in surface winds (Quan *et al.*, 2014; Herold *et al.*, 2012; Sherriff-Tadano *et al.*, 2018), resulting in low effective heat and moisture transfer to the continent at the eastern Atlantic margin. Moreover, a Mediterranean-type climate, dry in summer, had not yet been established (Quan *et al.*, 2014). The agreement between the Teruel $\delta^{18}O_c$ curve and SST and foraminiferal $\delta^{18}O$ datasets from ocean records at the same latitude and in the same climate band (Herbert *et al.*, 2016; Raymo *et al.*, 2018) increases from the Late Tortonian (~8.5 Ma), when the deep CAS waters disconnected (Molnar, 2008; Bell *et al.*, 2015). The AMOC system was then reinforced, and the current climatic dynamics and temperature gradients were established, with climate oscillations in western Europe being at least partially related to a situation of weaker or stronger AMOC (Fig. 11). At ~7.3 Ma, the subtropical high at mid-latitudes and the westerly belt reached their current position and from then on, the Atlantic conditions exerted a further influence on western Europe (Quan *et al.*, 2014; Herold *et al.*, 2012; Sherriff-Tadano *et al.*, 2018). From this point on, our data fit well with the SST variations in the Atlantic (Fig. 11).

A gradient is observed between Atlantic records from distinct latitudes (Fig. 11), with the ODP 608 record in the south (42°N) showing higher and more constant temperatures from the Late Tortonian to the Messinian, in line with the Teruel $\delta^{18}O_c$ data. Moreover, with increasing latitude, a general cooling tendency from 8 Ma until the end of the Late Messinian is more marked in the ocean records (Miller *et al*., 1991; Zachos *et al*., 2001; van Dam & Reichart, 2009; Herbert *et al*., 2016; Super *et al*., 2020). Between ~7 and 5.4 Ma (Late Miocene Cooling, LMC), the ocean water temperature dropped ~4ºC at a global scale at mid-latitudes (Turco *et al.*, 2001; Herbert *et al.*, 2016), and temperatures in the northern hemisphere were frequently poised near, but not below, the threshold for permanent continental ice formation (Herbert *et al*., 2016). Nevertheless, on the basis of $\delta^{13}C$ data, some authors propose that during the LMC several shorter warming events occurred related to temporary changes in the NADW (Bell *et al*., 2015; Otto-Bliesner *et al*., 2017). As previously expounded, our $\delta^{18}O_c$ record, like other climate datasets for the Iberian Peninsula (Fig. 10), suggests generally warm conditions in eastern Iberia from the Late Tortonian to the Zanclean. Even so, gentle excursions to lower $\delta^{18}O$ values (at ~7.1, ~6, and 5.3 to 5 Ma; Fig. 11) provide evidence of wetter-cooler periods in the region. These coincide with the decreases in temperature detected in the ODP 982, ODP 907, and Monte dei Corvi records (Fig. 11), suggesting that profound changes in the oceanic system could have had a clear effect on the SW Mediterranean area, even within warm climate conditions.

The subsequent recovery of the AMOC (Fig. 11) induced northern hemisphere warming in the Early Pliocene (Karas *et al.*, 2017), and the later weakening of the AMOC from ~3.8 to 3 Ma is in line with an Early Piacenzian global cooling trend and SST variations on a global scale (Fedorov *et al.*, 2013; Tzanova *et al.*, 2015; Herbert *et al.*, 2016). Both changes are recognized in our isotope curve, with increasing $\delta^{18}O_c$ values from 5.3 to 4.2 Ma in the Zanclean and decreasing values thereafter (Figs. 10 & 11). From the Piacenzian on, it is also evident that our $\delta^{18}O_c$ record shows lower values during weak AMOC stages (3.8-3 and 2.5-2.2 Ma) and higher values during strong AMOC episodes (3-2.5 and 2.2-2 Ma), which clearly evidences the influence of Atlantic dynamics on the climate of continental Iberia (Fig. 11).

In light of the foregoing, it can be stated that changes in the AMOC influence the climate of southwestern Europe mainly through modifications in the high-pressure centre in the mid-Atlantic (Fig. 12). Under a weak AMOC scenario and with a weakening of the Azores High, cold fronts from the Icelandic low-pressure system are allowed to sweep across the moderate latitudes of continental Europe. The resulting climate is cold and dry in northern Europe and wet in the Mediterranean area. It is proposed that under these conditions, an increasing P–E ratio and decreasing $\delta^{18}O$ precipitation values would induce lower $\delta^{18}O_c$ in our lacustrine record. Conversely, a pronounced Azores High would block westerly winds and storms, which would be diverted towards more northerly areas. As a consequence, aridity would increase in southwestern Europe, the P–E ratio would fall, and $\delta^{18}O$ precipitation values would increase; accordingly, higher $\delta^{18}O_c$ values were recorded in the Teruel record under this situation.

Considering the influence of the AMOC and eccentricity-induced modulation, two end-member scenarios can be envisaged (Fig. 12). During periods of strong AMOC and minimal eccentricity, the driest conditions would be reached, which would induce higher values of $\delta^{18}O_c$ (Fig. 12a). In contrast, during periods with weak AMOC and maximum eccentricity, the wettest conditions would be reached, which would imply lower values of $\delta^{18}O_c$ (Fig. 12b). The intermediate scenarios would correspond to values of $\delta^{18}O_c$ between the extremes. Moreover, the climate could have been modulated by the influence of shorter-order orbital cyclicity.

6. Conclusions

Climate changes impacted the continental systems of southwestern Europe at different scales during the Late Miocene-Early Pleistocene. The isotope signature of lacustrine carbonates in the Teruel Basin corroborates a relationship between $\delta^{18}O_c$ and the climate signal through the P–E ratio and a connection between dry and warm periods in this area of the western Mediterranean.

Orbital forcing controlled the climate conditions, and the relation between eccentricity and $\delta^{18}O_c$ values shows a correlation of eccentricity minima and maxima with dry and humid stages, respectively. The lacustrine record shows that the present-day connection between Atlantic dynamics and climate far from the coast in eastern Iberia already existed during the Late Miocene. The $\delta^{18}O_c$ curve agrees with North Atlantic sea-surface temperature curves, a connection existing between dry periods and high SST, which supports the influence of marine climate conditions landwards through heat and moisture transport from the Atlantic Ocean to the continent. A relation between climate changes in the region and marine isotope stages is also hypothesized. The effect of the closure of the Central Atlantic Seaway from ~8.6 Ma was to reinforce the warm/dry synchrony related to a stable high-pressure centre in the mid-Atlantic during strong AMOC stages. This diverted westerly winds northwards, increasing aridity in southwestern Europe.

The inferred warm/dry connection in the Teruel Basin, which differs from other western Mediterranean areas, supports previous interpretations proposing a regional climate gradient in western Europe, where warming and higher moisture have run parallel. The current paleogeographic configuration was established in the Late Miocene, the basin being located in an intramountainous area with an orographic barrier to the E-SE. As occurs at present, this situation would have isolated the study area from the influence of Mediterranean Sea humidity during warm periods, enhancing the Atlantic-continental connection.

The $\delta^{18}O_c$ curve presented here sheds substantial new light on the past climate in the western Mediterranean continental area and provides a powerful tool for other studies in eastern Iberia, especially of a paleontological or paleoecological nature. It is the longest paleoclimate record published and shows higher resolution than previous ones, helping to confirm past climate variations and fill information gaps between 9.8 and 1.8 Ma.

Acknowledgements

The authors would like to acknowledge the use of the Servicio General de Apoyo a la Investigación-SAI, Universidad de Zaragoza. This study was subsidized by the Agencia Estatal de Investigación (Ministerio de Ciencia e Innovación) of the Government of Spain (grant number PID2019-108705-GB-I00) and the Regional Government of Aragón (grant number E32_20R; research group *Geotransfer: Investigación Geológica* *para la Ciencia y la Sociedad*). We thank Rupert Glasgow who revised the English grammar. We would like to thank Prof. Jean-Pierre Suc and an anonymous reviewer for their useful comments and suggestions, which helped us improve the manuscript.

Abbreviations

AMOC– Atlantic Meridional Overturning Circulation
CAS – Central Atlantic Seaway
ELMA – European Land Mammal Age
ETWZ – European Temperate Wet Zone
GPTS – Geomagnetic Polarity Time Scale
LMC – Late Miocene Cooling
MAP – Mean Annual Precipitation
MAT – Mean Annual Temperature
MCO– Miocene Climate Optimum
mPWP – mid-Pliocene Warm Period
NADW – North Atlantic Deep Water
NAO – North Atlantic Oscillation
ODP – Ocean Drilling Program
P–E – Precipitation–evaporation
SHPZ – Subtropical High-Pressure Zone
SST – Sea Surface Temperature

Figure captions

Fig. 1. Deep Sea Drilling Program Map with the location of the Teruel Basin (red star) (inset shows the position of this intramountain basin in the eastern Iberian Range in Iberia). Selected sites from the Ocean Drilling Program (ODP) and Integrated Ocean Drilling Program (IODP), used in the discussion of the results (Figure 11) due to their proximity to the studied region, are also included (marked as black dots). MC refers to the Monte dei Corvi site.

Fig. 2. Geological context (**a**) and geological map (**b**) of the northern sector of the Teruel Basin.

Fig. 3. Composite stratigraphic profile of the northern Teruel Basin showing the calcite $\delta^{18}O_c$, $\delta^{13}C_c$, and mineralogical results. Lithologies are distinguished by colours: limestones and marls (blue, grey, and green), carbonated silts (purple), and mudstones (yellow). The anchoring with the chronostratigraphic time scale was based on magnetostratigraphic data and paleontological sites. The three climate periods proposed in this work are indicated.

Fig. 4. Field images of the lacustrine beds. **a.** Massive limestones in tabular-irregular strata (outcrop thickness ~20 m). **b.** Detail of the carbonate beds. **c.** Detail of the bioturbated tabular limestones.

Fig. 5. Field emission scanning electron microscope images (FESEM) of the limestones. Calcite crystals are in general small in size, with rhombohedral habits and common knobby surfaces consistent with neoformation.

Fig. 6. a. Qz + Phy and Cc correlation for the lacustrine samples from the Teruel Basin. **b.** Phy and Qz. **c.** Gy and Cc. **d.** Qz + Phy and Cc + Gy. Authigenic minerals such as calcite (Cc) and gypsum (Gy) show a negative linear relation with detrital minerals such as quartz (Qz) and phyllosilicates (Phy).

Fig. 7. $\delta^{18}O_c$ and $\delta^{13}C_c$ plots of the lacustrine carbonates in the Teruel Basin (blue dots) and the surrounding Mesozoic carbonate rocks (in black).

Fig. 8. a. Stable oxygen isotope ($\delta^{18}O_c$) curve of the Teruel Basin, spanning from ca. 9.8 to 1.8 Ma, calculated from lacustrine calcites; three broad/main climate periods are distinguished. **b.** Results from the spectral analysis (2σ MTM power spectrum with background AR(1) model and 95%, 99%, and 99.9% confidence levels) for the 66 to 209 m interval of the $\delta^{18}O$ time series and **c.** for the 140 to 209 m interval of the $\delta^{18}O$ time series. **d.** Tuned cyclostratigraphy for the filtered $\delta^{18}Oc$ time series and eccentricity curve calculated with the La2010a model (Gaussian filter passbands are 2.5 ± 0.5 and 0.4 ± 0.1). Tuning is based on assigning the pervasive 13.33 m cycle to the 405-ka eccentricity cycle. It is found that the most negative $\delta^{18}O_c$ values correlate with the maximum eccentricity of the Earth's orbit.

Fig. 9. COCO analysis and eCOCO sedimentation rate map of the $\delta^{18}Oc$ series in the Teruel profile (66-209 m). **a.** Composite stratigraphic profile for the northern Teruel Basin with calcite $\delta^{18}O_c$ and the Gaussian filter centred at 13.33 m (frequency = 0.075 ± 0.015) for the section used in the spectral analysis. **b.** The correlation coefficient

(top) and evolutionary correlation coefficient (bottom, coloured area). **c.** Null hypothesis test (top) and evolutionary null hypothesis (H_0) significance level (bottom). For both the COCO and eCOCO analyses, the tested sedimentation rates range from 1 to 10 cm/ka with a step of 0.1 cm/ka, and the number of Monte Carlo simulations is 2000. For the eCOCO analysis, the sliding window size is 35.75 m; the sliding window step is 1 m.

Fig. 10. Correlation of the $\delta^{18}O_c$ curve for the Teruel Basin with published climatic records for this basin and the east of the Iberian Peninsula. **a.** Our $\delta^{18}O_c$ curve with the periods of high and low aridity interpreted. **b.** Temperature/aridity curves based on micromammal associations in the Teruel Basin and other Neogene basins in Iberia. **c.** Temperature/aridity curves interpreted from the dentition record of macromammals in eastern Iberia. References are indicated in the figure. A comparison of the curves reinforces our proposal that low values of $\delta^{18}O_c$ indicate wet/cool periods and high $\delta^{18}O_c$ values indicate dry/warm periods.

Fig. 11. Correlation of the Teruel Basin $\delta^{18}O_c$ curve and other climate records. **a.** The $\delta^{18}O_c$ record reconstructed in this work as explained in Figure 3; the temporal position of some geological milestones is indicated. **b.** The $\delta^{18}O$ curve of deep marine benthic foraminifera. **c.** Selected curves of sea surface temperature (SST) and atmospheric pCO_2 changes inferred from North Atlantic Ocean and Mediterranean alkenone records. Previously proposed changes in the AMOC have been included. The references from which these data have been extracted are indicated. The MIS events as identified by Shackleton *et al.* (1995) and Lisiecki & Raymo (2005). Mi-glacials as established Abreu & Anderson (1998) and Wetershold *et al.* (2005).

Fig. 12. Synthesis of the possible scenarios involving eccentricity and AMOC overlapping during the studied time period.

References

Abels, H.A., Abdul Aziz, H., Ventra, D., & Hilgen F.J. (2009a). Orbital climate forcing in mudflat to marginal lacustrine deposits in the Miocene Teruel Basin (Northeast Spain). *Journal of Sedimentary Research,* 79, 831-847.

Abels, H.E., Abdul Aziz, H., Calvo, J.P., & Tuenter, E. (2009b). Shallow lacustrine carbonate microfacies document orbitally paced lake- level history in the Miocene Teruel Basin (North- East Spain). *Sedimentology,* 56, 399-419.

Abreu, V. & Anderson, J. (1998). Glacial Eustasy During the Cenozoic: Sequence Stratigraphic Implications. *AAPG Bulletin* 82. 1385-1400.

Alcalá, L., Alonso-Zarza, A.M., Álvarez, M.A., Azanza, B., Calvo, J.P., Cañaveras, J.C., van Dam, J.A., Garcés, M., Krijgsman, W., van der Meulen, A.J., Morales, J., Peláez, P., Pérez-González, A., Sánchez, S., Sancho, R. & Sanz, E. (2000). El registro sedimentario y faunístico de las cuencas de Calatayud-Daroca y Teruel. Evolución paleoambiental y paleoclimática durante el Neógeno. *Rev. Soc. Geol. España* 13, 323-343.

Alonso-Zarza, A.M., Calvo, J.P., van Dam, J. & Alcalá, L. (2000). Northern Teruel Graben Neogene, NE Spain. En: *Lake Basins Through Space and Time*. Gierlowski-Kordesch, F.H. y Kelts, K.R. (Eds.). Amer. Assoc. Petrol. Geol., Studies in Geology 46, 491-496.

Alonso-Zarza, A.M., Meléndez, A., Martín-García, R., Herrero, M.J. & Martín-Pérez, A. (2012). Discriminating between tectonism and climate signatures in palustrine deposits: Lessons from the Miocene of the Teruel Graben, NE Spain. *Earth-Science Reviews* 113, 141-160.

Álvaro, M., Capote, R. & Vegas, R. (1979). Un modelo de evolución geotectónica para la Cadena Celtibérica. *Acta Geológica Hispánica* 14, 172-177.

Andrews, J.E., Samways, G., Dennis, P.F., & Maher, B.A. (2000). Origin, abundance and storage of organic carbon and sulphur in the Holocene Humber Estuary: emphasizing human impact on storage changes, In: *Holocene Land-Ocean Interaction and Environmental Change Around the North Sea.* Shennan, I. y Andrews, J.E. (Eds.). Geological Society of London. 145-170.

Athanasiou, M., Athanasiou, M., Triantaphyllou, M., Dimiza, M., Gogou, A., & Theodorou G. (2015). Zanclean/Piacenzian transition on Cyprus (SE Mediterranean): calcareo us nannofossil evidence of sapropel formation. *Geo-Mar. Lett.*, 35, 367-385.

Barrón, E. Rivas-Carballo, R., Postigo Mijarra, J.M., Alcalde-Olivares, C., Vieira, M., Castro, L., Pais, J., &Valle-Hernández, M. (2010). The Cenozoic vegetation of the Iberian Peninsula: a synthesis. *Rev. Palaeobot. Palynol.*, 162, 382-402.

Bell, D.B., Jung, S., Kroon, D., Hodell, D.A., Lourens, L.J. & Raymo M.E. (2015). Atlantic Deep-water Response to the Early Pliocene Shoaling of the Central American Seaway. *Scientific Reports*, 5, 12252.

Benavente, C.A., Mancuso, A.C. & Bohacs, K.M. (2019). Paleohydrogeologic reconstruction of Triassic carbonate paleolakes from stable isotopes: Encompassing two lacustrine models. *Journal of South American Earth Sciences*, doi.org/10.1016/j.jsames.2019.102292

Bertini, A. (2001). Pliocene climatic cycles and altitudinal forest development from 2.7 Ma in the Northern Apennines (Italy): evidence from the pollen record of the Stirone section (c. 5.1 to c. 2.2 Ma). *Geobios* 34, 253–265.

Blanco, F., Gómez Cano, A.R., Cantalapiedra, J.L., Domingo, M.S., Domingo, L., Menéndez, I., Flynn, L.J., & Hernández Fernández, (2018). M. Differential responses of Miocene rodent metacommunities to global climatic changes were mediated by environmental context. *Scientific Reports*, 8, 2502.

Böhme, M., Ilg, A., & Winklhofer, M. (2008). Late Miocene "washhouse" climate in Europe. *Earth and Planetary Science Letters*, 275, 393-401.

Böhme, M., Winklhofer, M. & Ilg, A. (2011). Miocene precipitation in Europe: Temporal trends and spatial gradients. *Palaeogeography, Palaeoclimatology, Palaeoecology*, 304, 212-218.

Bruch, A.A. Utescher, T., Mosbrugger, V., & NECLIME members (2011). Precipitation patterns in the Miocene of Central Europe and the development of continentality. *Palaeogeography, Palaeoclimatology, Palaeoecology*, 304, 202–211.

Butiseaca, G. A., Vasiliev, I., Van der Meer, M., Krijgsman, W., Palcu, D., Feurdean, A., Niedermeyer, E. & Mulch, A. (2021). Severe late Miocene droughts affected western Eurasia. *Global and Planetary Change* 206, 103644.

Cabos N.W.D., de la Vara, A., Álvarez-García, F., Sanchez, E., Sieck, K., Pérez-Sanz, J.I., Limareva, N. & Sein, D. (2020). Impact of ocean-atmosphere coupling on regional climate: the Iberian Peninsula case. *Climate Dynamics* 54, 4441–4467.

Capote, R., Muñoz, J.A., Simón, J.L., Liesa, C.L. & Arlegui, L.E. (2002). Alpine tectonics I: The Alpine system north of the Betic Cordillera. In: *The Geology of Spain*. W. Gibbons y T. Moreno (Eds.). Geol. Soc. (London), 367-400.

Cerling, T., Harris, J., Macfadden, B., Lea-key, M., Quade, J., Eisenmann, V., Ehleringer, J. (1997). Global vegetation change through the Miocene/Pliocene boundary. *Nature*, 389, 153-158.

Chung, F.H. (1974). Quantitative interpretation of X-ray diffraction patterns of mixtures. II. Adiabatic principle of X-ray diffraction analysis of mixtures. *Journal of Applied Crystallography*, 7, 526-531.

Cleveland, W.S. (1979). Robust Locally Weighted Regression and Smoothing Scatterplots. *Journal of the American Statistical Association*, 74, 829-836.

Colás, J., Ramajo, J., Rosales, I., Armendáriz, M., Aurell, M., & Meléndez, G. (2010). *Análisis isotópico (δ18O y δ13C) del intervalo Calloviense-Oxfordiense en Tosos (Cordillera Ibérica): nuevos datos sobre la etapa de enfriamiento del final del Jurásico Medio.* In: Comunicaciones del V Congreso del Jurásico de España. J.I. Ruiz-Omeñaca, L. Piñuela y J.C. García-Ramos (Eds.). Museo del Jurásico de Asturias, Colunga 48.

Combourieu-Nebout, N., Foucault, A. & Mélières, F. (2004). Vegetation markers of paleoclimate cyclical changes in the Pliocene of Punta Piccola (Sicily, Italy). *Palaeogeography, Palaeoclimatology, Palaeoecology* 214, 55-66.

Craig, H. (1957). Isotopic standards for carbon and oxygen and correction factors for mass-spectrometric analysis of carbon dioxide. *Geochimica et Cosmochimica Acta*, 12, 133-149.

Craig, H. (1961). Isotopic variations in meteoric waters. *Science* 133, 1833-1834.

Ditlevsen, P. & Ashwin, P. (2018). Complex Climate Response to Astronomical Forcing: The Middle-Pleistocene Transition in Glacial Cycles and Changes in Frequency Locking. *Frontiers in Physics* 6. doi.org/10.3389/fphy.2018.00062.

De Miguel, D., Azanza, B., & Morales, J. (2019). Regional impacts of global climate change: a local humid phase in central Iberia in a late Miocene drying world. *Paleontology* 62, 77-92.

DeoCampo, D.M. (2010). The geochemistry of continental carbonates. In: *Carbonates in continental settings: geochemistry, diagenesis and applications: Developments in Sedimentology*. A.M., Alonso-Zarza y L.H., Tanner (Eds.). Elsevier, Amsterdam. 1-61.

De Schepper, S., Groeneveld, J., A Naafs, B.D., Van Renterghem, C., Hennissen, J., Head, M.J., Louwye, S., & Fabian, K. (2013). Northern Hemisphere Glaciation during the Globally Warm Early-Late Pliocene. *PLoS ONE*, 8(12), e81508.

Ditlevsen, P.D. & Ashwin, P. (2018). Complex Climate Response to Astronomical Forcing: The Middle-Pleistocene Transition in Glacial Cycles and Changes in Frequency Locking. *Front. Phys.* 6, 62.

Domingo, L. Grimes, S.T., Soledad, M., & Alberdi, M.T. (2009). Paleoenvironmental conditions in the Spanish Miocene-Pliocene Boundary: isotopic analyses of Hipparion dental enamel. *Naturwissenschaften*, 96, 503-511.

Domingo, L. Koch, P.L., Hernández-Fernández, M.L, Fox, D.L., Domingo, M.S., & Alberdi, M.T. (2013). Late Neogene and Early Quaternary Paleoenvironmental and Paleoclimatic Conditions in Southwestern Europe: Isotopic Analyses on Mammalian Taxa. *PLoS ONE* 8(5): e63739.

Donders, T.H., Weijers, J.W.H., Munsterman, D.K., Hoeve, M., Buckles, L.K., Pancost, R.D., Schouten, S., Sinninghe-Damste, J. & Brinkhuis, Henk. (2009). Strong climate coupling of terrestrial and marine environment in the Miocene of northwest Europe. *Earth and Planetary Sciences Letters* 281, 215-225.

Dorale, J.E.A.D. & Liu, Z.A.L. (2009). Limitations of Hendy Test Criteria for Judging the Paleocliamte suitability from speleothems and the need for replication. *Journal of Cave and Karst Studies* 1, 73-80.

Dowsett, H.J., Chandler, M.A., & Robinson, M.M. (2009). Surface temperatures of the Mid-Pliocene North Atlantic Ocean: Implications for future climate. *Phil. Trans. Roy. Soc. Am.,* 367, 69-84.

Dunagan, S.P. & Turner, C.E. (2004). Regional paleohydrologic and paleoclimatic settings of wetland/lacustrine depositional systems in the Morrison Formation (Upper Jurassic), Western Interior, USA. *Sedimentary Geology* 167, 269-296.

Edwards, E.J., Osborne, C.P., Strömberg, C.A., Smith, S.A., C4 Grasses Consortium, Bond, W.J., Christin, P.A., Cousins, A.B., Duvall, M.R., Fox, D.L., Freckleton, R.P., Ghannoum, O., Hartwell, J., Huang, Y., Janis, C.M., Keeley, J.E., Kellogg, E.A., Knapp, A.K., Leakey, A.D., Nelson, D.M., Saarela, J.M., Sage, R.F., Sala, O.E., Salamin, N., Still, C.J., & Tipple, B. (2010). The origins of C4 grasslands: integrating evolutionary and ecosystem science. *Science,* 328, 587-591.

Ehleringer, J.R., & Monson, R.K. (1993). Evolutionary and ecological aspects of photosynthetic pathway variation. *Ann. Rev. Ecolog. Syst.*, 24, 411-439.

Ezquerro, L. (2017). *El sector norte de la cuenca neógena de Teruel: tectónica, clima y sedimentación.* PhD Thesis, Universidad de Zaragoza, Zaragoza, 496 p. http://zaguan.unizar.es/record/77098#.

Ezquerro, L., Lafuente, P., Pesquero, Mª.D., Alcalá, L., Arlegui, L.E., Liesa, C.L., Luque, L. y Rodríguez-Pascua, M.A., Simón, J.L. (2012). Una cubeta endorreica residual plio-pleistocena en la zona de relevo entre las fallas de Concud y Teruel: implicaciones paleogeográficas. *Rev. Soc. Geol. Esp.* 25, 157-175.

Ezquerro, L., Luzón, A., Navarro, M., Liesa, C. L., & Simón, J.L. (2014). Climatic vs. tectonic signals in a continental extensional basin (Teruel, NE Spain) from stable isotope ($\delta^{18}O$) and sequence stratigraphical evolution. *Terra Nova,* 26, 337-346.

Ezquerro, L., Moretti, M., Liesa, C., Luzón, A., Pueyo, E.L. & Simón, J.L. (2016). Controls on space-time distribution of soft-sediment deformation structures: approaching the apparent recurrence period of paleoseisms at the Concud Fault (eastern Spain). *Sedimentary Geology* 344, 91-111.

Ezquerro, L., Luzón, A., Liesa, C.L. & Simón, J.L. (2019). Alluvial sedimentation and tectono-stratigraphic evolution in a narrow extensional zigzag basin margin (northern Teruel Basin, Spain). *J. Palaeogeogr.* 8, 29.

Ezquerro, L., Luzón, A., Simón, J.L. & Liesa, C. L. (2020). Segmentation and increasing activity in the Neogene-Quaternary Teruel Basin rift (Spain) revealed by morphotectonic approach. *Journal of Structural Geology,* 135, 104043.

Fauquette, S., Guiot, J. & Suc, J.P. (1998). A method for climatic reconstruction of the Mediterranean Pliocene using pollen data. *Palaeogeogr. Palaeoclimatol. Palaeoecol* 144, 183-201.

Fauquette, S., Suc, J.P., Guiot, J., Diniz, F., Feddi, N., Zheng, Z., Bessais, E. & Drivaliari, A. (1999). Climate and biomes in the West Mediterranean area during the Pliocene. *Palaeogeogr. Palaeoclimatol. Palaeoecol* 152, 15-36.

Fauquette, S., Suc, J.P., Bertini, A., Popescu, S.M., Warny, S. Bachiri-Taoufiq, N., Villa, M.J., Chikhi, H., Feddi, N., Subally, D., Clauzon, G. & Ferrier, J. (2006). How much did climate force the Messinian Salinity Crisis? Quantified climatic conditions from pollen records in the Mediterranean region. *Palaeogeography, Palaeoclimatology, Palaeoecology* 238, 281-301.

Fauquette, S., Suc, J.P., Jimé, G., Micheels, A., Jost, A., Favre, E., Bachiri-Taoufiq, N., Bertini, A., Clet-Pellerin, M, Diniz, F., Farjanel, G., Feddi, N., & Zheng, Z. (2007). Latitudinal climatic gradients in the Western European and Mediterranean regions from the Mid-Miocene (c. 15 Ma) to the Mid-Pliocene (c. 3.5 Ma) as quantified from pollen data. In: *Deep-Time Perspectives on Climate Change: Marrying the Signal from Computer Models and Biological Proxies*. M. Williams, A.M. Haywood, J. Gregory & D.N. Schmidt (Eds.) The Micropalaeontological Society, Special Publications. The Geological Society, London, 481–502.

Fedorov, A., Brierley, C.M., Lawrence, K.T., Liu, Z., Dekens, P.S., & Ravelo, A.C. (2013). Patterns and mechanisms of early Pliocene warmth. *Nature*, 496, 43-49.

Fortelius, M. Eronen, J., Liu, L., Pushkina, D., Tesakov, A., Vislobokova, I., Zhang, Z. (2006). Late Miocene and Pliocene large land mammals and climatic changes in Eurasia. *Palaeogeography Palaeoclimatology Palaeoecology* 238, 219-227.

Garcés, M., Krijgsman, W., Van Dam, J., Calvo, J.P., Alcalá, L. y Alonso-Zarza, A.M. (1999). Late Miocene alluvial sediments from the Teruel area: Magnetostratigraphy, magnetic susceptibility, and facies organization. *Acta Geológica Hispánica* 32, 171-184.

García-Alix, A., Minwer-Barakat, R., Martín-Suárez, E., Freudenthal, M. & Martín, J.M. (2008). Late Miocene–Early Pliocene climatic evolution of the Granada Basin (southern Spain) deduced from the paleoecology of the micromammal associations. *Palaeogeography, Palaeoclimatology, Palaeoecology* 265, 214-225.

Godoy, A., Moissenet, E., Ramírez, J.I., Olivé, A., Aznar, J.M., Jerez Mir, L., Aragonés, E., Aguilar, M.J., Ramírez del Pozo, J., Leal, M.C., Adrover, R., Alberdi, M.T., Giner, J., Gutiérrez Elorza, M., Portero, J.M. & Gabaldón, V. (1983a). *Mapa Geológico de España 1:50.000, hoja nº 542 (Alfambra).* IGME, Madrid.

Godoy, A., Ramírez, J.I., Olivé, A., Moissenet, E., Aznar, J.M., Aragonés, E., Aguilar, M.J., Ramírez del Pozo, J., Leal, M.C., Jerez Mir, L., Adrover, R., Goy, A., Comas, M.J., Alberdi, M.T., Giner, J., Gutiérrez Elorza, M., Portero, J.M. & Gabaldón, V. (1983b). *Mapa Geológico de España 1: 50.000, hoja nº 567 (Teruel)*. IGME, Madrid.

Gonfiantini, R. (1984). *Report of Advisory Group Meeting on stable isotope reference samples for geochemical and hydrological investigations.* International Atomic Energy Agency, Vienna.

Griffin, D.L. (2002). Aridity and humidity: two aspects of the late Miocene climate of North Africa and the Mediterranean, *Palaeogeography, Palaeoclimatology, Palaeoecology*, 182, 65-91.

Grygar, T. M., Hošek, M., Mach, K., Schnabl, P. & Martinez, M. (2017). Climatic instability before the Miocene Climatic Optimum reflected in a Central European lacustrine record from the Most Basin in the Czech Republic. *Palaeogeography, Palaeoclimatology, Palaeoecology*, 485, 930-945.

Haug, G.H., Hughen, K.A., Sigman, D.M., Peterson, L.C., & Rohl, U. (2001). Southward migration of the Intertropical Convergence Zone through the Holocene. *Science*, 293, 1304-1308.

Haywood, A.M., Chandler, M.A., Valdes, P.J., Salzmann, U., Lunt, D.J., & Dowsett, H.J. (2009). Comparison of mid-Pliocene climate predictions produced by the HadAM3 and GCMAM3 General Circulation Models. *Glob. Planet. Change*, 66, 208-224.

Haywood, A.M., Dowsett, H. J., & Dolan, A.M. (2016). Integrating geological archives and climate models for the mid-Pliocene warm period, *Nature Communication.*, 7, doi:10.1038/ncomms10646

Herbert, D.T. Lawrence, K.T., Tzanova, A., Peterson, L.C., Caballero-Gill, R.P., & Kelly, C.S. (2016). Late Miocene global cooling and the rise of modern ecosystems. *Nature Geoscience*, 9, 843–847.

Hernández, A., Trigo, R.M., Pla-Rabes, S., Valero-Garcés, B.L., Jerez, S., Rico-Herrero, M., Vega, J.C., Jambrina-Enríquez, M., & Giralt, S. (2015). Sensitivity of two Iberian lakes to North Atlantic atmospheric circulation modes. *Climate Dynamics*, 45, 3403–3417.

Hernández Fernández, M., Álvarez-Sierra, Á. & Peláez-Campomanes, P. (2007). Bioclimatic analysis of rodent palaeofaunas reveals severe climatic changes in Southwestern Europe during the Plio-Pleistocene. *Palaeogeography, Palaeoclimatology, Palaeoecology* 251, 500-526.

Herold, N., Huber, M., Müller, R.D., & Seton, M. (2012). *Modeling the Miocene Climatic Optimum: Ocean Circulation.* Department of Earth, Atmospheric, and Planetary Sciences Faculty Publications, paper 180.

Hodell, D.A., & Woodruff, F. (1994). Variations in the strontium isotopic ratio of seawater during the Miocene: stratigraphic and geochemical implications. *Paleoceanography*, 9, 405–426.

Hoefs, J. (2009). *Stable* Isotope *Geochemistry*. Springer-Verlag, Berlin. 285 p.

Holbourn, A.E., Kuhnt, W., Clemens, S.C., Joehnck, J., Lübbers, J., Kochhann, K.G.D., & Andersen, N. (2018). Late Miocene climate cooling and intensification of southeast Asian winter monsoon. *Nature Communications*, 9, 1584.

Ivanovic, R.F., Valdes, P.J., Gregoir, L., Flecker, R., & Gutjahr, M. (2014). Sensitivity of modern climate to the presence, strength and salinity of Mediterranean-Atlantic exchange in a global general circulation model. *Climate Dynamics*, 42, 859–877.

Jiménez-Moreno, G., Fauquette, S., & Suc, J.P. (2008). Vegetation, climate and palaeoaltitude reconstructions of the Eastern Alps during the Miocene based on pollen records from Austria, Central Europe. *Journal of Biogeography* 35, 1638-1649.

Jiménez-Moreno, G., Suc, J.P. & Fauquette, S. (2010). Miocene to Pliocene vegetation reconstruction and climate estimates in the Iberian Peninsula from pollen data. *Rev. Palaeobot. Palynol.* 162, 403–415.

Jiménez-Moreno, G., Burjachs, F., Expósito, I., Oms, O., Carrancho, A., Villalain, J.J., van der Made, J., Agustí, J., Campeny, G. & Gómez de Soler, B. (2013). Late Pliocene vegetation and orbital-scale climate changes from the western Mediterranean area. *Glob. Planet. Chang.* 108, 15–28.

Jiménez-Moreno, G., Pérez-Asensio, J., Larrasoaña, J., Sierro, F., Garcia-Castellanos, D., Salazar, A., Salvany, J., Ledesma-Mateo, S., Mata, M.P. & Mediavilla, C. (2019). Early Pliocene climatic optimum, cooling and early glaciation deduced by terrestrial and marine environmental changes in SW Spain. *Global and Planetary Change* 180, 89-99.

Jones, M.D. & Roberts, C.N. (2008). Interpreting lake isotope records of Holocene environmental change in the Eastern Mediterranean. Quaternary International 181, 32-38

Karas, C., Nürnberg, D., Bahr, A., Groeneveld, J., Herrle, J.O., Tiedemann, R., & deMenocal, P.B. (2017). Pliocene oceanic seaways and global climate. *Scientific Reports*, 7, 39842. doi:10.1038/srep39842

Krijgsman, W., Garcés, M., Langereis, C. G., Daams, R., van Dam, J., van der Meulen, A.J., Agustí, J., & Cabrera, L. (1996). A new chronology for the middle to late Miocene continental record in Spain. *Earth and Planetary Science Letters*, 142, 367-380.

Laskar, J., Fienga, A., Gastineau, M., & Manche, H. (2011). La2010: a new orbital solution for the long-term motion of the Earth. *Astronomy & Astrophysics*, 532, A89

Lawrence K.T., Sosdian, S., White, H.E., & Rosenthal, Y. (2010). North Atlantic climate evolution through the Plio-Pleistocene climate transitions. *Earth and Planetary Science Letters*, 300. 329–342.

Leng, M.J., & Marshall, J.D. (2004). Palaeoclimate interpretation of stable isotope data from lake sediment archives. *Quaternary Science Reviews*, 23, 811-831.

Lear, C.H., Rosenthal, Y., & Wright, J.D. (2003). The closing of a seaway: Ocean water masses and global climate change. *Earth Planet. Sci. Lett.*, 210, 425-436.

Li, H.C. & Ku, T.L. (1997). $\delta^{13}C$-$\delta^{18}O$ covariance as a palaeohydrological indicator for closed-basin lakes. *Palaeogeography, Palaeoclimatology, Palaeoecology* 132, 69-80.

Li, M., Hinnov, L., & Kump, L. (2019). Acycle: Time-series analysis software for paleoclimate projects and education, *Computers & Geosciences*, 127, 12-22.

Liesa, C.L., Simón, J.L., Ezquerro, L., Arlegui, L.E. & Luzón, A., (2019). Stress evolution and structural inheritance controlling an intracontinental extensional basin: The central-northern sector of the Neogene Teruel Basin. *Journal of Structural Geology* 118, 362-376.

Lindsay, E., Fahlbusch, V., & Mein, P. (1989). *European Neogene Mammal Chronology*. NATO ASI Series. 658 p.

Lisiecki, L.E. & Raymo, M.E. (2005) A Pliocene-Pleistocene stack of 57 globally distributed benthic ^{18}O records. *Paleoceanography* 20, PA1003.

Lohmann, G., Butzin, M., & Bickert, T. (2015). Effect of Vegetation on the Late Miocene Ocean Circulation. *Journal of Marine Science and Engineering*, 3, 1311-1333.

Luzón, A., Mayayo, M.J.; Pérez, A. (2009). Stable isotope characterisation of co-existing carboantes from the Holocene Gallocanta lake (NE Spain): paleolimnological implications. *International Journal of Earth Sciences* 98, 11209-1150.

Luzón, A., Gauthier, A., Pérez, A., Pueyo-Anchuela, O., Mayayo, M.J. & Muñoz, A. (2017). Late Pleistocene-Holocene palaeoenvirontmental evolution of the Añamara River valley (Iberian Range, NE Spain): Multidisciplinary approach on the study of carbonate fluvial deposists. *Quaternary International* 437, 51-70.

Mangini, A., Blumbach, P., Verdes, P., Spötl, C., Scholz, D., Machel, H. & Mahon, S. (2007). Combined records from a stalagmite from Barbados and from lake sediments in Haiti reveal variable seasonality in the Caribbean between 6.7 and 3 ka BP. *Quaternary Science Reviews* 26, 1332-1343.

Martín-Suárez, E., Freudenthal, M. & Civis, J. (2001). Rodent palaeoecology of the Continental Upper Miocene of Crevillente (Alicante, SE Spain). *Palaeogeography, Palaeoclimatology, Palaeoecology* 165, 349–356.

Matson, S.D., & Fox, D. (2010). Stable isotopic evidence for terrestrial latitudinal climate gradients in the Late Miocene of the Iberian Peninsula. *Palaeogeography, Palaeoclimatology, Palaeoecology*, 287, 28 – 44.

McCrea, J.M. (1950). The isotopic composition of carbonates and a paleotemperature scale. *Journal of Chemical Physics*, 18, 849-857.

Mein, P. (1975). Resultats du Groupe de Travail des Vertebres. *Report on activity of the R.C.M.N.S. Working groups*, Bratislava, 77-81.

Mein, P., Moissenet, E., & Adrover, R., (1990). Biostratigraphie du Néogène supérieur de Teruel. *Paleontología i Evolució*, 23, 121-139.

Methner, K., Campani, M., Fiebig, J., Löffler, N., Kempf, O. & Mulch, A. (2020). Middle Miocene long-term continental temperature change in and out of pace with marine climate records. *Scientific Reports* 10. 10.1038/s41598-020-64743-5.

Meyers, S.R. & Hinnov, L.A. (2010), Northern Hemisphere glaciation and the evolution of Plio- Pleistocene climate noise. *Paleoceanography* 25, PA3207.

Moissenet, E. (1980). Relief et déformations récentes: trois transversales dans les fossés internes des Chaînes Ibériques orientales. *Rév. Géograph. Pyrénées et Sud-Ouest*, 51 (3), 315-344.

Moissenet, E. (1983). Aspectos de la neotectónica en la fosa de Teruel. In: *Libro Jubilar, J.M. Ríos. Geología de España, Tomo 2*. Comba J.A. (Ed.). IGME, Madrid, 427-446.

Molnar, P. (2008). Closing of the Central American Seaway and the Ice Age: A critical review. *Paleoceanography*, 23, PA2201, doi:10.1029/2007PA001574

Moreno, A., Sancho, C., Bartolomé, M., Oliva-Urcia, B., Delgado-Huertas, A., Estrela, M.J., Corell, D., López-Moreno, J.I., & Cacho, I. (2014). Climate controls on rainfall isotopes and their effects on cave drip water and speleothem growth: the case of Molinos cave (Teruel, NE Spain). *Climate Dynamics*, 43, 221–241.

Moreno, A., Iglesias, M., Azorin-Molina, C., Pérez-Mejías, C., Bartolomé, M., Sancho, C., Stoll, H., Cacho, I., Frigola, J., Osácar, C., Muñoz, A., Delgado-Huertas, A., Bladé, I., and Vimeux, F.: Measurement report: Spatial variability of northern Iberian rainfall stable isotope values – investigating atmospheric controls on daily and monthly timescales, Atmos. Chem. Phys., 21, 10159–10177.

Mosbrugger, V., Utescher, T., & Dilcher, D. (2005). Cenozoic continental climatic evolution of Central Europe. *Proc. Natl. Acad. Sci.*, 102, 14964-14969.

Ogg, J.G. Chapter 5: geomagnetic polarity time scale. In: *The Geologic Time Scale*. Gradstein, F.M., Ogg, J.G., Schmitz, M.D. y Ogg, G.M. (Eds.). Elsevier, Amsterdam (2012).

Oliva-Urcia, B. & Moreno, A. (2019). Discerning the major environmental processes that influence the magnetic properties in three northern Iberia mountain lakes. Catena, 182, 104130.

Opdyke, N., Mein, P., Lindsay, E., Pérez-González, A., Moissenet, E., & Norton, V.L., (1997). Continental deposits, magnetostratigraphy and vertebrate paleontology, late Neogene of Eastern Spain. *Palaeogeography, Palaeoclimatology, Palaeoecology,* 133, 129-148.

Otto-Bliesner, B., Jahn, A., Feng, R., Brady, E., Hu, A., & Marcus, L. (2017). Amplified North Atlantic warming in the late Pliocene by changes in Arctic gateways. *Geophys. Res. Lett.*, 44, 957–964.

Pagani, M., Liu, Z.H., LaRiviere, J., & Ravelo, A.C. (2010). High Earth-system climate sensitivity determined from Pliocene carbon dioxide concentrations. *Nature Ge~~i~~oscience*, 3, 27-30.

Pearson, P.N., & Palmer, M.R. (2000). Atmospheric carbon dioxide concentrations over the past 60 million years. *Nature*, 406, 695-699.

Pellegrino, L., Dela Pierre, F., Natalicchio, M., & Carnevale, G. (2018). The Messinian diatomite deposition in the Mediterranean region and its relationships to the global silica cycle. *Earth-Science Reviews* 178, 154-176.

Pérez-Asensio, J., Aguirre, J., Schmiedl, G. & Jorge, C. (2012). Impact of restriction of the Atlantic-Mediterranean gateway on the Mediterranean Outflow Water and eastern Atlantic circulation during the Messinian. *Paleoceanography* 27, 1-14.

Pérez-Mejías, C., Sancho, C., Gázquez, F., Moreno, A., Bartolomé, M., Osácar, M.C., & Cheng, H. (2018). Transference of isotopic signal from rainfall to dripwaters and farmed calcite in Mediterranean semi-arid karst. *Geochimica et Cosmochimica Acta*, 243, 66-98.

Pla-Pueyo, S., Viseras, C., Candy, I., Soria, J.M., García-García, F. & Schreve, D. (2015). Climatic control on palaeohydrology and cyclical sediment distribution in the Plio-Quaternary deposits of the Guadix Basin (Betic Cordillera, Spain). *Quat. Int.* 389, 56–69.

Postigo-Mijarra, J.M., Barrón, E., Gómez-Manzaneque, F., & Morla, C. (2009). Floristic changes in the Iberian Peninsula and Balearic Islands (SW Europe) during the Cenozoic. *J. Biogeogr.*, 36, 2025-2043.

Potter, P.E., & Szatmari, P. (2009). Global Miocene tectonics and the modern world. *Earth-Sci. Rev.*, 96, 279-295.

Prista, G., Agostinho, R. & Cachão, M. (2015). Observing the past to better understand the future: A synthesis of the Neogene climate in Europe and its perspectives on present climate change. *Journal of Geosciences* 7, 65-83.

Quade, J., Chivas, A.R. & McCulloch, M.T. (1995). Strontium and carbon isotope tracers and the origins of soil carbonate in South Australia and Victoria. *Palaeogeography, Palaeoclimatology, Palaeoecology* 113, 103-117.

Quade, J., Garzione, C. & Eiler, J. (2007). Paleoelevation reconstruction using pedogenic carbonates. *Rev. Mineral. Geochem.* 66, 53–87.

Quan, C., Liu, Y.S.C., Tang, H., & Utescher, T. (2014) Miocene shift of European atmospheric circulation from trade wind to westerlies. *Scientific Reports*, 4, 5660, doi: 10.1038/srep05660.

Raymo, M.E., Kozdon, R., Evans, D., Lisiecki, L., & Ford, H.L. (2018). The accuracy of mid-Pliocene $\delta^{18}O$-based ice volume and sea level reconstructions. *Earth-Science Review*, 177, 291-302.

Ribera d'Alcalà, M. (2019). Similarities, differences and mechanisms of climate impact on terrestrial vs. marine ecosystems. In: *Italian Long-Term Ecological Research for understanding ecosystem diversity and functioning. Case studies from aquatic, terrestrial and transitional domains*. Mazzocchi, M.G., Capotondi, L., Freppaz, M., Lugliè, A. & Campanaro, A. (Eds). Nature Conservation 34, 505–523.

Rietveld, H.M. (1969). A Profile Refinement Method for Nuclear and Magnetic Structures. *Journal of Applied Crystallography*, 2, 65-71.

Rodríguez-López, J.P., Liesa, C.L., van Dam, J., Lafuente, P., Arlegui, L., Ezquerro, L. & de Boer, P.L. (2012). Aeolian construction and alluvial dismantling of a fault-bounded intracontinental aeolian dune field (Teruel Basin, Spain); a continental perspective on late Pliocene climate change and variability. *Sedimentology*, 55, 1253-1292.

Seki, O., Foster, G.L., Schmidt, D.N., Mackensen, A., Kawamura, K., & Pancost, R.D. (2010). Alkenone and boron-based Pliocene pCO_2 records. *Earth and Planetary Science Letters*, 292, 201–211.

Shackleton, N.J., Hall, M.A. & Pate, D. (1995). Pliocene stable isotope stratigraphy of Site 864. *In: Pisias, NG; Mayer, LA; Janecek, TR; Palmer-Julson, A; van Andel, TH (eds.), Proceedings of the Ocean Drilling Program, Scientific Results, College Station, TX (Ocean Drilling Program)*, 138, 337-355.

Sherriff‐Tadano, S., Abe-Ouchi, A., Yoshimori, M., Oka, A., & Chan, W. (2018). Influence of glacial ice sheets on the Atlantic meridional overturning circulation through surface wind change. *Clim. Dyn.*, 50, 2881–2903.

Simón, J.L. (1986). Analysis of a gradual change in stress regime (example from the eastern Iberian Chain, Spain). *Tectonophysics* 124, 37–53.

Simón, J.L., Arlegui, L.E., Lafuente, P. & Liesa, C.L. (2012). Active extensional faults in the central eastern Iberian Chain, Spain. *Journal of Iberian Geology* 38, 127-144.

Stap, L.B., de Boer, B., Ziegler, M., Bintanja, R., Lourens, L.J., & Roderik, S.W. (2016). CO_2 over the past 5 million years: Continuous simulation and new δ^{11}B-based proxy data. *Earth and Planetary Science Letters*, 439, 1-10.

Stuiver, M. (1970). Oxygen and carbon isotope ratios of fresh-water carbonates as climatic indicators. *Journal of Geophysical Research* 75, 5247-5257.

Suc, J.L.P. (1978). Analyse pollinique de depost plio – pleistocenes du sud du Massif basaltique de l'Escandorgue (serie de Bernasso - Lunas, Herault - France). *Pollen er spores*, 20. 4, 497-512.

Suc, J.P. (1984). Origin and evolution of the Mediterranean vegetation and climate in Europe. *Nature* 307, 429-432.

Suc, J.P., Fauquette, S., Bessedik, M., Bertini, A., Zheng, Z., Clauzon, G., Suballyova, D., Diniz, F., Quézel, P., Feddi, N., Clet, M., Bessais, E., Bachiri Taoufiq, N., Méon, H., & Combourieu-Nebout, N. (1999). Neogene vegetation changes in West European and West circum-Mediterranean areas. In: *Hominid Evolution and Climate in Europe, Climatic and Environmental Change in the Neogene of Europe*. Agustí, J., Rook, L. & Andrews P. (Eds.). Cambridge University Press. 370-385.

Suc, J.P., Popescu, S.M., Fauquette, S., Bessedik, M., Jiménez-Moreno, G., Bachiri-Taoufiq, N., Zheng, Z., Médail, F. & Klotz, S. (2018). Reconstruction of Mediterranean flora, vegetation and climate for the last 23 million years based on an extensive pollen dataset. *Ecologia mediterranea* 44, 53-85.

Talbot, M.R. (1990). A review of the palaeohydrological interpretation of carbon and oxygen isotopic ratios in primary lacustrine carbonates. *Chemical Geology (Isotope Geoscience Section)* 80, 261-279.

Teranes, J.L., & McKenzie J.A. (2001). Lacustrine oxygen isotope record of 20th-century climate change in central Europe: Evaluation of climatic controls on oxygen isotopes in precipitation. *J. Paleolimnol.*, 26, 131-146.

Thiede, J., Winkler, A., Wolf-Welling, T., Eldholm,O., Myhre, A.M., Baumann, K.H., Henrich, R., & Stei, R. (1998). Late Cenozoic history of the polar north Atlantic: results from ocean drilling. *Quaternary Science Reviews*, 17, 185-208.

Thomson, D.J. (1982). Spectrum estimation and harmonic analysis. *Proceedings of the IEEE*, 70, 1055–1096.

Tuel, A., & Eltahir, E. A. B. (2020). Why Is the Mediterranean a Climate Change Hot Spot?, *Journal of Climate 33*, 5829-5843.

Tuenter, E. (2004). *Modeling Orbital Induced Variations in Circum-Mediterranean Climate*. PhD thesis, Utrecht University, 152 p.

Turco, E., Hilgen, F., Lourens, L., Shackleton, N.J., & Zachariasse, J.W. (2001). Punctuated evolution of global climate cooling during the late Middle to early late Miocene: high-resolution planktonic forminiferal and oxygen isotope records from the Mediterranean. *Paleoceanography*, 16 (4), 405-423.

Tzanova, A., Herbert, T., & Peterson, L. (2015). Cooling Mediterranean Sea surface temperatures during the Late Miocene provide a climate context for evolutionary transitions in Africa and Eurasia. *Earth and Planetary Science Letters*, 419, 71-80.

Utescher, T., Mosbrugger, V., & Ashraf, A.R. (2000). Climate evolution in Northwest Germany over the last 25 million years. *Palaios*, 15, 430-449.

Utescher, T., Ashraf, A.R., Dreist, A., Dybkjær, K., Mosbrugger, V., Pross, J. & Wilde, V. (2012). Variability of Neogene continental climates in Northwest Europe - a detailed study based on microfloras. *Turkish Journal of Earth Sciences*, 21, 289-314.

Val, J., Bádenas, B., Aurell, M., & Rosale, I. (2017). Cyclostratigraphy and chemostratigraphy of a bioclastic storm dominated carbonate ramp (late Pliensbachian, Iberian Basin). *Sedimentary Geology* 355, 93-113.

Valero Garces, B.L., Gierlowski-Kordesch, E. & Bragonier, W.A. (1997). Pennsylvanian continental cyclothem development: no evidence of direct climate control in the Upper Freeport Formation (Allegheny Group) of Pennsylvania (northern Appalachian Basin). *Sedimentary Geology*, 109, 305-319.

van Dam, J.A. (2006). Geographic and temporal patterns in the late Neogene (12–3 Ma) aridification of Europe: The use of small mammals as paleoprecipitation proxies. *Palaeogeography, Palaeoclimatology, Palaeoecology*, 238, 190-218.

van Dam, J.A., & Weltje, G.J. (1999). Reconstruction of the late Miocene climate of Spain using rodent paleocommunity successions: an application of end-member modelling. *Palaeogeogr. Palaeoclimatol. Palaeoecol.*, 151, 267–305.

van Dam, J.A., Abdul Aziz, H., Álvarez Sierra, M.A., Hilgen, F.J., van den Hoek Ostende, L.W., Lourens, L.J., Mein, P., van der Meulen, A.J., & Pelaez-Campomanes, P. (2006). Long-period astronomical forcing of mammal turnover. *Nature letters*, 443, 687-691.

van Dam, J.A., & Reichart, G. J. (2009). Oxygen and carbon isotope signatures in Late Neogene horse teeth from Spain and application as temperature and seasonality proxies. *Palaeogeography, Palaeoclimatology, Palaeoecology*, 274, 64-81

Walters, L.J. Jr., Caypool, G.G., & Choquette, P.W. (1972). Reaction rates and ^{18}O variation for the carbonate-phosphoric acid preparation method. *Geochimica Cosmochimica Acta*, 36, 129-140.

Wang, X., Auler, A. S., Edwards, R. L., Cheng H., Ito, E., & Solheid, M. (2006). Interhemispheric anti-phasing of rainfall during the last glacial period. *Quat. Sci. Rev.*, 25, 3391-3403.

Weerd, A. van de (1976). *Rodent faunas of the Mio-Pliocene continental sediments of the Teruel-Alfambra region, Spain*. Utrecht Micropaleontology Bulletin, Special Publication 2, 217 p.

Westerhold, T., Bickert, T. & Röhl, U. (2005). Middle to Late Miocene oxygen isotope stratigraphy of ODP site 1085 (SE Atlantic): New constrains on Miocene climate variability and sea-level fluctuations. *Palaeogeography, Palaeoclimatology, Palaeoecology* 217. 205-222.

Winkler, A., Wolf-Welling, T., Stattegger, K. & Thiede, J. (2002). Clay mineral sedimentation in high northern latitude deep-sea basins since the Middle Miocene (ODP Leg 151, NAAG). *Int J Earth Sci*, 91, 133–148.

Zachos, J. Pagani, M., Sloan, L., Thomas, E., & Billups, K. (2001). Trends, rhythms, and aberrations in global climate 65 Ma to present. *Science*, 292, 686–693.

Zhang, Z., Nisancioglu, K.H., Chandler, M.A., Haywood, A.M., Otto-Bliesner, B.L., Ramstein, G., Stepanek, C., Abe-Ouchi, A., Chan, W.L., Bragg, F.J., Contoux, C., Dolan, A.M., Hill, D.J., Jost, A., Kamae, Y., Lohmann, G., Lunt, D.J., Rosenbloom, N.A., Sohl, L.E., & Ueda, H. (2013). Mid-pliocene Atlantic Meridional Overturning Circulation not unlike modern. *Clim. Past*., 9, 1495–1504.

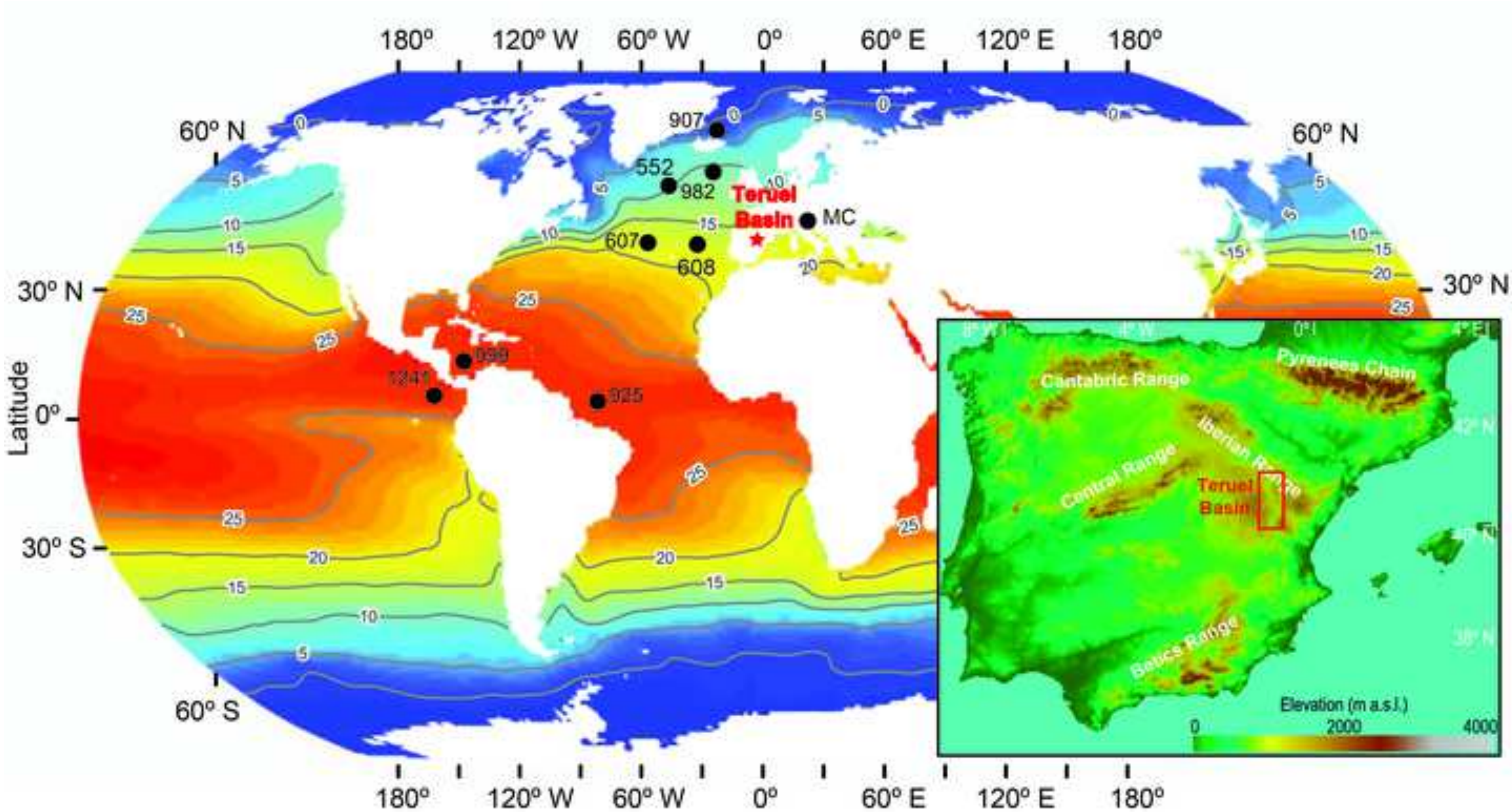
180º
120º W
60º W
0º
60º E
120º E
180º
60º N
30º N
0º
30º S
60º S
Latitude
907
552
982
607
608
MC
1241
999
925
Teruel Basin
Cantabric Range
Pyrenees Chain
Iberian Range
Central Range
Betics Range
Teruel Basin
Elevation (m a.s.l.)
0
2000
4000

Figure 2

Click here to access/download;Figure;Fig. 2.jpg

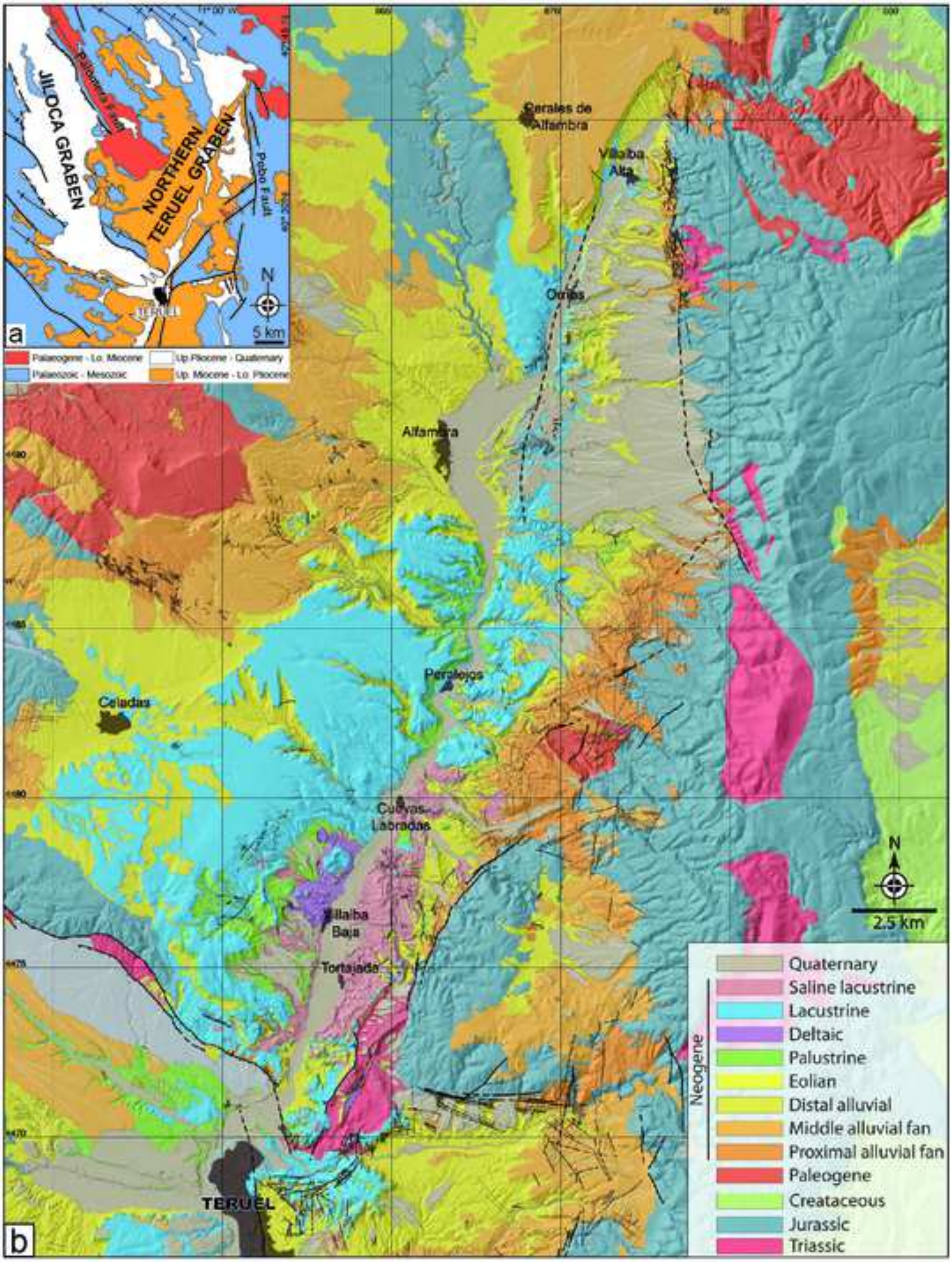

Figure 7

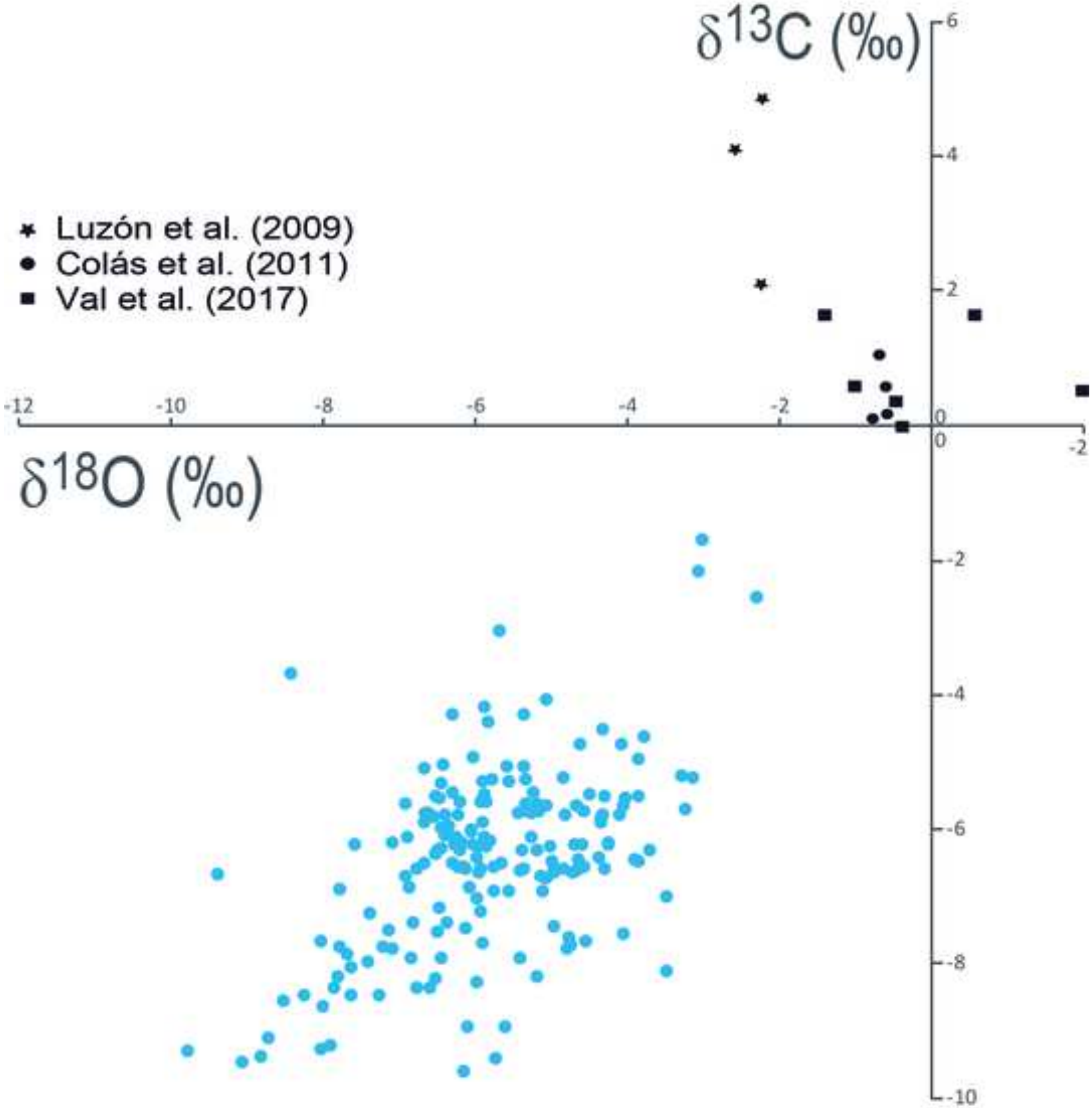
δ13C (‰)
δ18O (‰)
Luzón et al. (2009)
Colás et al. (2011)
Val et al. (2017)
-12
-10
-8
-6
-4
-2
0
-2
6
4
2
0
-2
-4
-6
-8
-10

Figure 8

Click here to access/download;Figure;Fig. 8.jpg

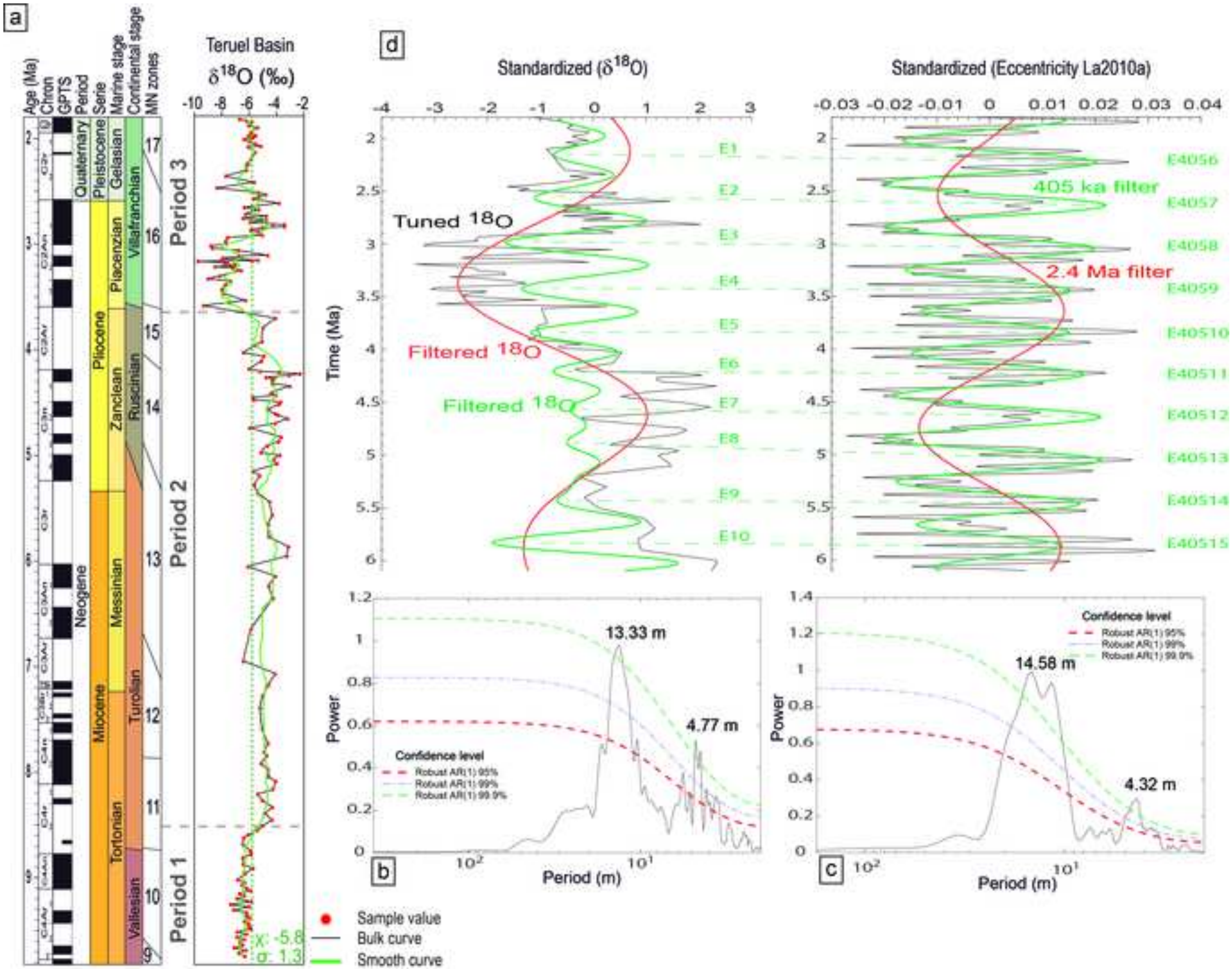

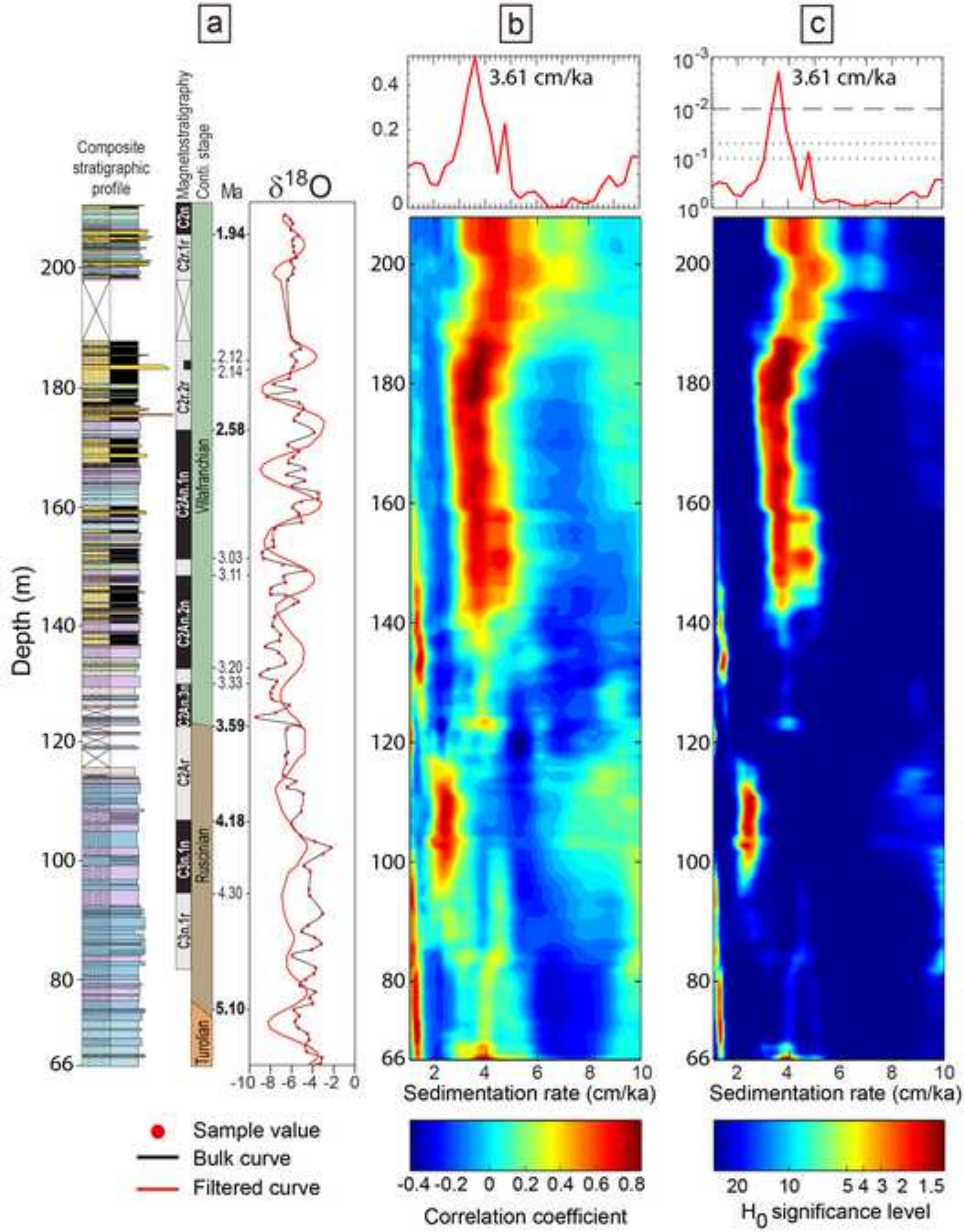
a
b
c
Composite stratigraphic profile
Magnetostratigraphy
Conti. stage
Ma
δ18O
Depth (m)
Villafranchian
Ruscinian
Turolian
3.61 cm/ka
3.61 cm/ka
Sedimentation rate (cm/ka)
Sedimentation rate (cm/ka)
Sample value
Bulk curve
Filtered curve
Correlation coefficient
H0 significance level

Figure 10

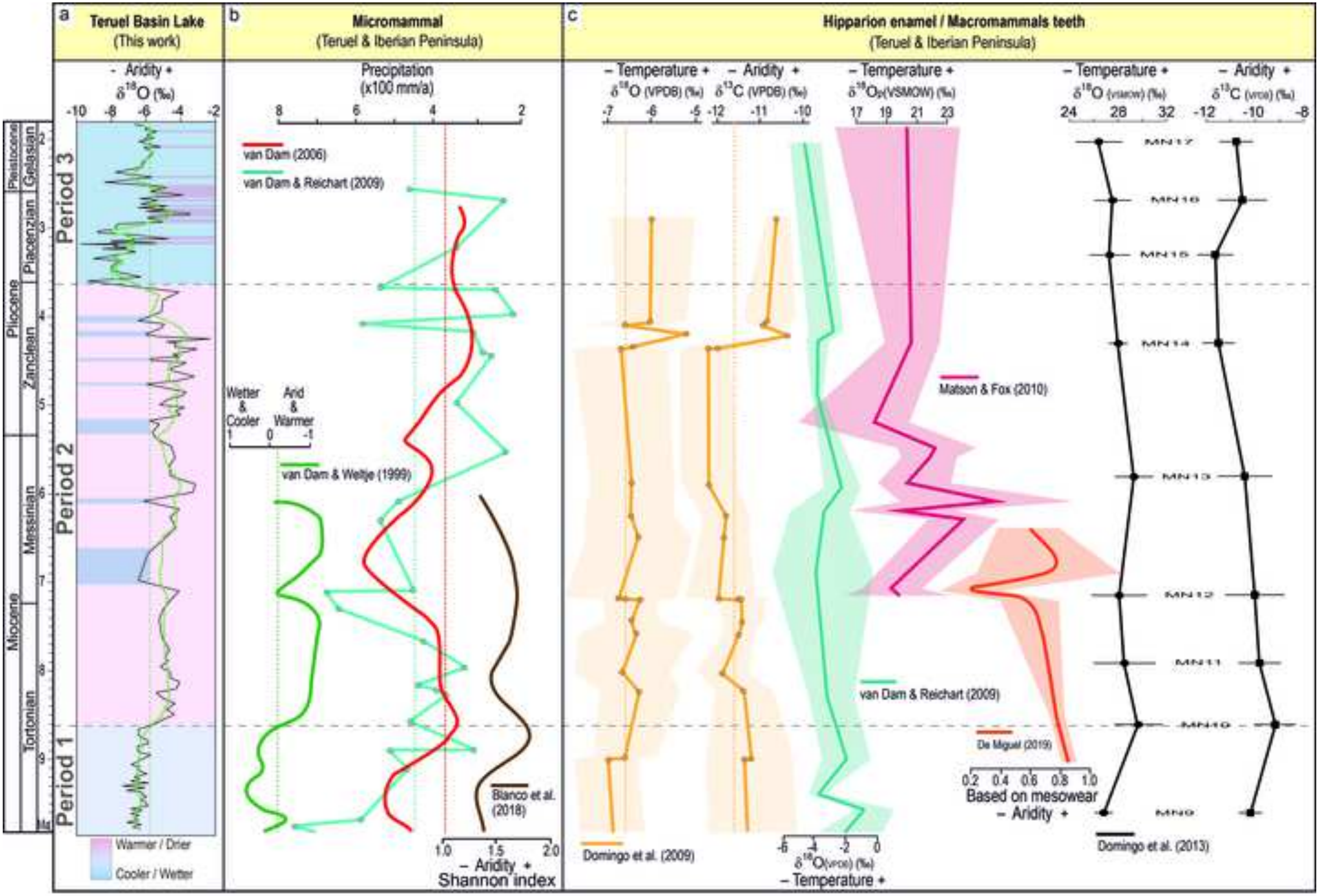
a
Teruel Basin Lake
(This work)
- Aridity +
δ18O (‰)
Pleistocene
Gelasian
Piacenzian
Pliocene
Zanclean
Messinian
Miocene
Tortonian
Ma
Period 3
Period 2
Period 1
Warmer / Drier
Cooler / Wetter
b
Micromammal
(Teruel & Iberian Peninsula)
Precipitation
(x100 mm/a)
van Dam (2006)
van Dam & Reichart (2009)
Wetter & Cooler
Arid & Warmer
van Dam & Weltje (1999)
Blanco et al. (2018)
– Aridity +
Shannon index
c
Hipparion enamel / Macromammals teeth
(Teruel & Iberian Peninsula)
– Temperature +
δ18O (VPDB) (‰)
– Aridity +
δ13C (VPDB) (‰)
δ18Op(VSMOW) (‰)
δ18O (VSMOW) (‰)
δ13C (VPDB) (‰)
Matson & Fox (2010)
van Dam & Reichart (2009)
De Miguel (2019)
Based on mesowear
– Aridity +
Domingo et al. (2009)
δ18O(VPDB) (‰)
– Temperature +
Domingo et al. (2013)
MN17
MN16
MN15
MN14
MN13
MN12
MN11
MN10
MN9

Figure 11

Click here to access/download;Figure;Fig. 11.jpg